

Efficient Sampling Allocation Strategies for General Graph-Filter-Based Signal Recovery

Lital Dabush *Student Member, IEEE* and Tirza Routtenberg, *Senior Member, IEEE*

Abstract—Sensor placement plays a crucial role in graph signal recovery in underdetermined systems. In this paper, we present the graph-filtered regularized maximum likelihood (GFR-ML) estimator of graph signals, which integrates general graph filtering with regularization to enhance signal recovery performance under a limited number of sensors. Then, we investigate task-based sampling allocation aimed at minimizing the mean squared error (MSE) of the GFR-ML estimator by wisely choosing sensor placement. Since this MSE depends on the unknown graph signals to be estimated, we propose four cost functions for the optimization of the sampling allocation: the biased Cramér-Rao bound (bCRB), the worst-case MSE (WC-MSE), the Bayesian MSE (BMSE), and the worst-case BMSE (WC-BMSE), where the last two assume a Gaussian prior. We investigate the properties of these cost functions and develop two algorithms for their practical implementation: 1) the straightforward greedy algorithm; and 2) the alternating projection gradient descent (PGD) algorithm that reduces the computational complexity. Simulation results on synthetic and real-world datasets of the IEEE 118-bus power system and the Minnesota road network demonstrate that the proposed sampling allocation methods reduce the MSE by up to 50% compared to the common sampling methods A-design, E-design, and LR-design in the tested scenarios. Thus, the proposed methods improve the estimation performance and reduce the required number of measurements in graph signal processing (GSP)-based signal recovery in the case of underdetermined systems.

Index Terms—Regularized estimation; graph signal processing (GSP); graph filters; network observability; sensor allocation

I. INTRODUCTION

Modern complex systems in fields such as engineering, physics, biology, and sociology often generate signals supported on irregular structures, naturally modeled as graph signals [1]. These signals, indexed by the graph vertices, have spurred the development of graph signal processing (GSP), which generalizes classical digital signal processing (DSP) theory to data on graphs [2]–[4]. Graph signal recovery aims to estimate graph signals from noisy, corrupted, or incomplete measurements. Applications include data registration across sensor networks [5], time synchronization in distributed networks [6], [7], and state estimation in power systems [5], [8]–[12]. The recovery performance highly depends on the sensor placement [13]. Efficient sampling is essential to managing large, complex datasets [2], [3], as raw data processing consumes significant computational and storage resources. GSP-based sampling strategies that retain essential information for the graph signal recovery task while reducing data size are, therefore, highly desirable.

Research on the sampling and recovery of graph signals has increased significantly in recent years [14]–[18]. Sampling methods can generally be divided into random

and deterministic approaches [19]. In random sampling, we select nodes (vertices) randomly according to a probability distribution, often designed to prioritize “important”/central nodes [20]–[23]. These methods are computationally efficient and easily implemented in a distributed manner, but generally require more samples than deterministic approaches in order to achieve comparable reconstruction quality, even for bandlimited signals [19]. In contrast, deterministic sampling aims to optimize sensor placement by minimizing a cost function, typically related to the processing task that will be conducted with the sampled graph signals. As signal recovery is usually an ill-posed inverse problem, regularized or constrained optimization is commonly used to incorporate additional information and improve performance [5], [15], [17]–[19], [24]–[27].

Most sampling methods for graph signals rely on specific assumptions, such as bandlimitedness or smoothness, to enable recovery. Bandlimited graph signals, commonly assumed in GSP, can achieve perfect recovery under experimental sampling design, as demonstrated in prior work [14], [16]. Various sampling policies were developed for this case, including the A-optimality criterion (A-design) approach [14], fast distributed algorithms [15], [26], local weighted measurements [17], local aggregation [18], and percolation from seeding nodes [27]. However, all these methods are constrained to graph signals that are strictly bandlimited, which may restrict their applicability. The less restrictive smoothness assumption on the graph signals has been utilized for the sampling approach, for example, via Laplacian regularization [2], [5], [19], [24], [25], [28]. However, while smoothness can describe many realistic scenarios, it still imposes restrictive conditions, as not all graph signals are smooth with respect to (w.r.t.) the graph [16], [29].

In [30], a smooth observation model was considered, and the Laplacian-regularized sampling allocation (LR-design) was proposed to minimize the largest eigenvalue of the estimator’s coefficient matrix. However, these works considered specific graph filters for the observation and the regularization.

Sampling methods that do not assume specific graph signals include, for example, an approach wherein one learns a sparse dictionary representation of the signals [29]. However, this method requires a large amount of data in order to learn the dictionary. Other sampling techniques assume general measurement models, such as those in [31]–[33]; [32] and [33] additionally incorporate the minimization of the Cramér-Rao bound (CRB) to address the dependency on the unknown variable to be estimated. Nevertheless, these methods do not utilize GSP formulations or tools, such as graph filters or common regularization techniques. However, using the graph filtering measurement model and general regularization has the potential to enable a robust sampling and recovery framework with enhanced estimation performance across a broader range of graph signal types and applications.

In this paper, we investigate task-based sampling for the

Lital Dabush and Tirza Routtenberg are with the School of Electrical and Computer Engineering Ben-Gurion University of the Negev Beer-Sheva 84105, Israel, e-mail: litaldab@post.bgu.ac.il, tirzar@bgu.ac.il.

This research was supported by the ISRAEL SCIENCE FOUNDATION (Grant No. 1148/22) and by the Israel Ministry of National Infrastructure and Energy. L. Dabush is a fellow of the AdR Women Doctoral Program.

estimation of graph signals. First, we introduce the graph filter regularized (GFR)-maximum likelihood (ML) estimator, which integrates general graph filtering as a regularization for graph signal recovery. In order to optimize the sampling scheme, the mean-squared-error (MSE) of the GFR-ML estimator is a natural objective function. However, we show that this MSE is a function of the unknown parameters, making direct optimization impractical. Thus, we develop sampling allocation strategies based on four cost functions designed to optimize sensor placement in the estimation accuracy sense: (i) the non-Bayesian biased CRB (bCRB) (with the bias of the GFR-ML estimator); (ii) the worst-case MSE (WC-MSE); (iii) the Bayesian MSE (BMSE); (iv) and the worst-case BMSE (WC-BMSE). To minimize these cost functions, we propose two practical algorithms: a greedy algorithm that provides an efficient ad-hoc solution; and an alternating projected gradient descent (PGD) algorithm that solves the convex relaxation of the sampling allocation problem, providing a computationally efficient solution. As a byproduct of the alternating PGD algorithm, we derive the gradients of all cost functions for general graph filters, offering a versatile and scalable sampling allocation framework for general graph signals. Simulation results on synthetic and real-world datasets, including the IEEE 118-bus power system [34] and the Minnesota road network [35], demonstrate that the proposed sampling allocation methods significantly reduce the MSE compared to the standard sampling strategies A-design [14], experimentally designed sampling (E-design) [16], and LR-design [30].

The remainder of the paper is organized as follows. In Section II, we provide background on GSP. Section III describes the model, the estimation approach, and the considered sampling allocation problem. In Section IV, we propose and analyze different cost functions for the sampling approach: the bCRB, WC-MSE, BMSE, and WC-BMSE approaches. In Section V, we present a greedy algorithm and alternating PGD algorithm for efficient sensor selection. Section VI presents our simulation study. Finally, the conclusions are provided in Section VII.

In the rest of this paper, vectors and matrices are denoted by boldface lowercase letters and boldface uppercase letters, respectively. The notations $(\cdot)^T$, $(\cdot)^{-1}$, $(\cdot)^\dagger$, and $\text{tr}(\cdot)$ denote the transpose, inverse, Moore-Penrose pseudo-inverse, and trace operators, respectively. The m th element of the vector \mathbf{a} and the (m, q) th element of the matrix \mathbf{A} are denoted by a_m and $A_{m,q}$, respectively. The parameters λ_i , $\lambda_{\min}(\mathbf{A})$ and $\lambda_{\max}(\mathbf{A})$ denote the i th, the minimum and the maximum eigenvalues of the matrix \mathbf{A} , respectively. The gradient of a scalar function $g(\mathbf{a}) \in \mathbb{R}$ w.r.t. the vector $\mathbf{a} \in \mathbb{R}^{M \times 1}$ is denoted by $\nabla_{\mathbf{a}} g(\mathbf{a}) \in \mathbb{R}^{M \times 1}$. The Jacobian of a vector function $\mathbf{g}(\mathbf{a}) \in \mathbb{R}^{K \times 1}$ w.r.t. \mathbf{a} is denoted by $\nabla_{\mathbf{a}} \mathbf{g}(\mathbf{a}) \in \mathbb{R}^{K \times M}$, where each entry is defined as $[\nabla_{\mathbf{a}} \mathbf{g}(\mathbf{a})]_{m,k} = \frac{\partial g_m(\mathbf{a})}{\partial a_k}$. \mathbf{I} , and $\mathbf{1}$ and $\mathbf{0}$ denote the identity matrix, and vectors of ones and zeros, respectively, with appropriate dimensions, and $\|\cdot\|$ denotes the Euclidean l_2 -norm of a vector. For a vector \mathbf{a} , $\mathcal{P}_{\mathcal{C}}(\mathbf{a})$ denotes the projection of \mathbf{a} onto the set \mathcal{C} , and $\text{diag}(\mathbf{a})$ is a diagonal matrix whose (m, m) th entry is a_m .

II. BACKGROUND: GRAPH SIGNAL PROCESSING (GSP)

Let $\mathcal{G}(\mathcal{V}, \xi)$ be a general undirected weighted graph, where $\mathcal{V} = \{1, \dots, N\}$ and ξ are the sets of nodes and edges, respectively. The matrix $\mathbf{W} \in \mathbb{R}^{N \times N}$ is the weighted adjacency

matrix of the graph $\mathcal{G}(\mathcal{V}, \xi)$, where $W_{k,n} \geq 0$ denotes the weight of the edge between node k and node n , and $W_{k,n} = 0$ if no edge exists between k and n . The graph Laplacian matrix,

$$\mathbf{L} \triangleq \text{diag}(\mathbf{W}\mathbf{1}) - \mathbf{W}, \quad (1)$$

is a real positive semi-definite matrix with the eigenvalue decomposition (EVD) defined as

$$\mathbf{L} = \mathbf{V} \text{diag}(\boldsymbol{\lambda}) \mathbf{V}^{-1}, \quad (2)$$

where the columns of \mathbf{V} are the eigenvectors of \mathbf{L} , $\mathbf{V}^T = \mathbf{V}^{-1}$, and $\boldsymbol{\lambda} \in \mathbb{R}^N$ is a vector of the ordered eigenvalues of \mathbf{L} in decreasing order. We assume that $\mathcal{G}(\mathcal{V}, \xi)$ is a connected graph, and thus, $\lambda_2 \neq 0$ [1]. By analogy to the frequency of signals in DSP, the Laplacian eigenvalues, $\lambda_1, \dots, \lambda_N$, can be interpreted as the graph frequencies. Together with the eigenvectors in \mathbf{V} , they define the spectrum of the graph [2].

A graph signal is a function that resides on a graph, assigning a scalar value to each node. The graph Fourier transform (GFT) of a graph signal $\mathbf{a} \in \mathbb{R}^N$ w.r.t. the graph $\mathcal{G}(\mathcal{V}, \xi)$ is defined as [2], [3]

$$\tilde{\mathbf{a}} \triangleq \mathbf{V}^{-1} \mathbf{a}. \quad (3)$$

Similarly, the inverse GFT is obtained by a left multiplication of $\tilde{\mathbf{a}}$ by \mathbf{V} . The total variation (TV) of a graph signal \mathbf{a} satisfies

$$\mathbf{a}^T \mathbf{L} \mathbf{a} = \frac{1}{2} \sum_{k=1}^N \sum_{n=1}^N W_{k,n} (a_k - a_n)^2 = \sum_{n=1}^N \lambda_n \tilde{a}_n^2, \quad (4)$$

where the first equality is obtained by substituting (1), and the second equality is obtained by substituting (2) and (3).

The TV from (4) is a smoothness measure, which is used in graphs to quantify changes w.r.t. the variability that is encoded by the weights of the graph [2], [36]. A graph signal, \mathbf{a} , is smooth if $\mathbf{a}^T \mathbf{L} \mathbf{a} \leq \varepsilon$, where ε is small in terms of the specific application [2]. Thus, the smoothness assumption implies that neighboring nodes have similar values, and the graph signal spectrum is in the small eigenvalues region (see (4)).

Linear and shift-invariant graph filters play essential roles in GSP. These filters generalize linear time-invariant filters used in DSP, and enable processing over graphs [2], [4]. A Laplacian-based graph filter can be defined in the graph frequency domain as a function $h(\cdot)$ that allows an EVD [4]:

$$h(\mathbf{L}) \triangleq \mathbf{V} \text{diag}(h(\boldsymbol{\lambda})) \mathbf{V}^{-1}, \quad h(\boldsymbol{\lambda}) = [h(\lambda_1), \dots, h(\lambda_N)], \quad (5)$$

where $h(\lambda_n)$ is the graph filter frequency response at the graph frequency λ_n , $n = 1, \dots, N$. The graph filter frequency response should be identical for all equal eigenvalues (see, e.g. [25], Chapter 3). A graph filter applied on a graph signal is a linear operator that satisfies the following:

$$\mathbf{a}^{(\text{out})} = h(\mathbf{L}) \mathbf{a}^{(\text{in})}, \quad (6)$$

where $\mathbf{a}^{(\text{out})}$ and $\mathbf{a}^{(\text{in})}$ are the output and input graph signals. Following DSP conventions, low-pass graph filters (graph LPFs) are filters that do not significantly affect the frequency content of low-frequency signals but attenuate the magnitude of high-frequency signals. Analogously, high-pass graph filters (graph HPFs) pass high-frequency signals while attenuating low frequencies [3].

III. MODEL, ESTIMATORS, AND PROBLEM FORMULATION

In this section, we describe the sampling allocation problem in GSP-based models with the goal of enhancing estimation performance. First, we introduce the measurement model in Subsection III-A. Then, we derive the GFR-ML estimator associated with this model in Subsection III-B. Finally, we formulate the sampling allocation problem associated with the estimation performance in Subsection III-C.

A. GSP Measurement Model

We consider a linear graph filtering model:

$$\mathbf{y} = h_M(\mathbf{L})\mathbf{x} + \mathbf{e}, \quad (7)$$

where $\mathbf{y} \in \mathbb{R}^N$ and $\mathbf{x} \in \mathbb{R}^N$ are the output and input graph signals, respectively. The vector $\mathbf{e} \in \mathbb{R}^N$ represents a zero-mean Gaussian noise with covariance matrix \mathbf{R} , i.e. $\mathbf{e} \sim \mathcal{N}(\mathbf{0}, \mathbf{R})$. The graph filter, $h_M(\mathbf{L}) \in \mathbb{R}^{N \times N}$, and the graph topology represented by \mathbf{L} are assumed to be known. The input graph signal, \mathbf{x} , is unknown and needs to be estimated. The model described in (7) is well-established in GSP and has been applied in various applications [3], [19], [37]–[40]. This model effectively captures how signals propagate over network structures, leveraging graph filters to represent signal behavior dictated by underlying graph topologies [2].

In practice, resource constraints such as budget, energy, and maintenance often limit the number of sensors deployed in large networks [13], [19], [37], since sensor deployment incurs significant costs, including initial investment and ongoing expenses for data transmission and power supply. To model this situation, let $\mathcal{S} \subseteq \mathcal{V}$ denote the subset of sampled nodes, where \mathcal{V} is the set of all nodes with $|\mathcal{V}| = N$. The measurement model from (7) under this setting of partial observations is

$$\mathbf{y}_S = [h_M(\mathbf{L})]_{S,\mathcal{V}}\mathbf{x} + \mathbf{e}_S, \quad (8)$$

where $\mathbf{y}_S \in \mathbb{R}^{|\mathcal{S}|}$ represents the observed measurements at the sampled nodes, and $\mathbf{e}_S \in \mathbb{R}^{|\mathcal{S}|}$ is the corresponding noise vector. The notation $[h_M(\mathbf{L})]_{S,\mathcal{V}}$ denotes the sub-matrix of $h_M(\mathbf{L})$ containing the rows indexed by \mathcal{S} , which correspond to the sampled nodes. An alternative formulation uses a sampling indicator vector $\mathbf{d} \in \{0, 1\}^N$, where $d_n = 1$ if the n th node is sampled and $d_n = 0$ otherwise. Then, the partial measurement model from (8) can be written as

$$\mathbf{D}\mathbf{y} = \mathbf{D}h_M(\mathbf{L})\mathbf{x} + \mathbf{D}\mathbf{e}, \quad (9)$$

where $\mathbf{D} = \text{diag}(\mathbf{d})$.

For the system in (8) (or, equivalently, (9)) to yield a unique solution for \mathbf{x} in the least squares sense even in the noiseless scenario, the matrix $[h_M(\mathbf{L})]_{S,\mathcal{V}}(\mathbf{D}h_M(\mathbf{L}))$ must be full row rank. Otherwise, the system is underdetermined, and additional information is needed to obtain a unique solution for \mathbf{x} . As mentioned above, a common approach in GSP to address this issue is to assume that the graph signals are smooth or have low TV. To extend this assumption to other types of graph signals beyond low-pass or smooth signals, we introduce a constraint w.r.t. a general semi-definite graph filter $h_R^+(\mathbf{L}) \in \mathbb{R}^{N \times N}$, i.e. we assume

$$\mathcal{E}_L(\mathbf{x}) = (\mathbf{x} - \mathbf{x}_0)^T h_R^+(\mathbf{L})(\mathbf{x} - \mathbf{x}_0) \leq \varepsilon, \quad (10)$$

where ε is a tolerance parameter, and $\mathbf{x}_0 \in \mathbb{R}^N$ is a reference signal. The generalized regularization in (10), in the context

of a general graph HPF, $h_R^+(\mathbf{L})$, and without \mathbf{x}_0 , is presented in [23] and on p. 132 of [25]. The inclusion of \mathbf{x}_0 extends the scenario where \mathbf{x} is near the kernel of $h_R^+(\mathbf{L})$ to cases with another general reference point, \mathbf{x}_0 . This is particularly useful when $h_R^+(\mathbf{L})$ is a full-rank matrix, and thus, only the zero vector lies in its kernel.

Discussion on the generalized graph filter regularization in (10): The assumption in (10) generalizes several commonly-used priors. For example, setting $\mathbf{x}_0 = c\mathbf{1}$, where $c \in \mathbb{R}$, and $h_R^+(\mathbf{L}) = \mathbf{L}$ corresponds to the traditional smoothness prior, which has been widely used in various applications (see, e.g. [5], [19], [24], [25], [28]). Similarly, bandlimited graph signals that are limited to a subset of graph frequencies, $\mathcal{R} \subset \mathcal{V}$, and are widely used in GSP [3], [41]–[45], can be modeled by setting $\mathbf{x}_0 = \sum_{i \in \mathcal{R}} a_i \mathbf{v}_i$, where $a_i \in \mathbb{R}$, and defining $h_R^+(\mathbf{L})$ to eliminate frequencies outside of \mathcal{R} , i.e. $h_R^+(\mathbf{L}) = \mathbf{V} \text{diag}(\mathbf{1}_{\{\mathcal{V} \setminus \mathcal{R}\}}) \mathbf{V}^{-1}$, where $\mathbf{1}_{\{A\}}$ denotes the indicator function for the event A .

These priors are widely used in diverse applications. In image processing, \mathbf{x} denotes pixel intensities, and \mathbf{L} is defined by the pixel adjacency. The prior $\mathbf{x}^T \mathbf{L} \mathbf{x} \leq \varepsilon$ enforces smoothness, aiding in denoising and reconstruction [2], [23]–[25]. In semi-supervised learning, \mathbf{x} can represent label scores, with \mathbf{L} encoding data similarity. A prior of the form $(\mathbf{x} - \mathbf{x}_0)^T \mathbf{L} (\mathbf{x} - \mathbf{x}_0)$ smoothly propagates labels, improving classification accuracy [2], [4]. In power systems, where \mathbf{x} represents the states (voltages) and \mathbf{L} corresponds to the admittance matrix, the prior in (10) imposes smoothness with \mathbf{x}_0 as a reference voltage and $h_R^+(\mathbf{L})$ is any graph HPF [5], [9]. Similarly, in sensor networks, small variations w.r.t. the graph can be exploited for fault detection using high-pass filtering of graph signals [3].

Another interpretation of the prior in (10) is from a Bayesian estimation perspective, where the input graph signal, \mathbf{x} , is random and has a Gaussian distribution [46], [47]:

$$\mathbf{x} \sim \mathcal{N}(\mathbf{x}_0, \frac{1}{\mu} (h_R^+(\mathbf{L}))^\dagger), \quad (11)$$

where μ scales the variance of the signal. The log-likelihood of this prior (up to constant) is $\mu(\mathbf{x} - \mathbf{x}_0)^T h_R^+(\mathbf{L})(\mathbf{x} - \mathbf{x}_0)$, which can be added as a regularization term.

B. The GFR-ML Estimator

To incorporate the prior in (10) into the estimation process, we formulate an optimization problem that combines the likelihood function of the measurement vector from (9) with the constraint from (10). The resulting estimator is obtained by solving the following optimization problem:

$$\hat{\mathbf{x}} = \arg \min_{\mathbf{x} \in \mathbb{R}^N} \|\mathbf{D}(\mathbf{y} - h_M(\mathbf{L})\mathbf{x})\|_{\mathbf{R}^{-1}}^2 + \mu \|h_R^+(\mathbf{L})(\mathbf{x} - \mathbf{x}_0)\|^2, \quad (12)$$

where the operator $\|\mathbf{z}\|_{\mathbf{A}}^2 \triangleq \mathbf{z}^T \mathbf{A} \mathbf{z}$ denotes the quadratic form of the matrix \mathbf{A} , and $\mu > 0$ is a regularization parameter that balances the data fidelity term with the prior.

Solving the optimization problem in (12) leads to a regularized ML estimator, named here the GFR-ML estimator, for the recovery of \mathbf{x} . Since the objective in (12) is a convex function of \mathbf{x} , by equating the derivative of (12) w.r.t. \mathbf{x} to zero (see, e.g. p. 17 in [48]), we obtain

$$\hat{\mathbf{x}} = \mathbf{K}^{-1}(\mathbf{d})(h_M^T(\mathbf{L})\mathbf{D}\mathbf{R}^{-1}\mathbf{D}\mathbf{y} + \mu h_R^+(\mathbf{L})\mathbf{x}_0), \quad (13)$$

where

$$\mathbf{K}(\mathbf{d}) \triangleq h_{\mathbf{M}}^T(\mathbf{L})\mathbf{D}\mathbf{R}^{-1}\mathbf{D}h_{\mathbf{M}}(\mathbf{L}) + \mu h_{\mathbf{R}}^+(\mathbf{L}). \quad (14)$$

It should also be noted that for the Bayesian perspective described in (11), the estimator in (13)-(14) is also the minimum MSE (MMSE) estimator.

The term $\mu h_{\mathbf{R}}^+(\mathbf{L})$ ensures that $\mathbf{K}(\mathbf{d})$ can be positive definite and invertible, even for underdetermined systems, where $|\mathcal{S}| < N$ and $h_{\mathbf{M}}^T(\mathbf{L})\mathbf{D}\mathbf{R}^{-1}\mathbf{D}h_{\mathbf{M}}(\mathbf{L})$ is a rank-deficient matrix. This regularization allows for a unique solution and incorporates prior knowledge into the estimation process. The GFR-ML estimator uses graph filters, given by $h_{\mathbf{M}}$ and $h_{\mathbf{R}}^+$, in both the measurement model and the regularization term. Unlike estimators that rely solely on Laplacian-based regularization, it employs the flexibility of general graph filters via $h_{\mathbf{R}}^+(\mathbf{L})$, enabling adaptation to specific structural and spectral properties, such as bandlimitedness and task-specific frequency weighting.

Furthermore, as both the measurement model $h_{\mathbf{M}}(\mathbf{L})$ and the regularization term $h_{\mathbf{R}}^+(\mathbf{L})$ are graph filters, these filters can be efficiently approximated or implemented as finite impulse response (FIR) graph filters. Specifically, when $h_{\mathbf{M}}(\mathbf{L})$ and $h_{\mathbf{R}}^+(\mathbf{L})$ are modeled as polynomial graph filters [25], i.e. $h_{\mathbf{M}}(\mathbf{L}) = \sum_{k=0}^K h_k \mathbf{L}^k$ and $h_{\mathbf{R}}^+(\mathbf{L}) = \sum_{k=0}^P f_k \mathbf{L}^k$, the matrix-vector multiplications required for the estimator involve only localized computations, where each node processes information from its immediate neighbors. For further efficiency, Chebyshev polynomial approximations [24] can be employed to reduce computational complexity. These properties allow for scalable, distributed implementations, making the GFR-ML estimator particularly suitable for large-scale networks.

C. Problem Formulation - Sampling Allocation

Sensor locations have a significant impact on the estimation performance in various applications (see, e.g. [13], [49]). We assume a constrained amount of sensing resources, $\sum_n d_n = q$, e.g. due to limited energy and communication budget. This requirement can be rewritten as the constraint $\|\mathbf{d}\|^2 = q$. Thus, the sampling task can be written as

$$\mathbf{d}^{opt} = \arg \min_{\mathbf{d} \in \{0,1\}^N: \|\mathbf{d}\|^2 = q} C(\mathbf{d}), \quad (15)$$

where $C(\mathbf{d})$ denotes a general cost function that is associated with the estimation performance. Alternatively, if the number of sensors to be selected, i.e. q , is unknown, we can reformulate the sensor selection problem to minimize the number of nonzero entries in \mathbf{d} rather than fixing q as in (15). This approach yields the number of selected sensors as a byproduct, as follows:

$$\begin{aligned} \mathbf{d}^{opt} &= \arg \min_{\mathbf{d} \in \{0,1\}^N} \|\mathbf{d}\|^2 \\ \text{s.t. } & C(\mathbf{d}) \leq \varepsilon. \end{aligned} \quad (16)$$

As our goal is to minimize the MSE of the GFR-ML estimator, the natural choice for $C(\mathbf{d})$ is the MSE of this non-Bayesian estimator, $\hat{\mathbf{x}}$, given by

$$\text{MSE}(\hat{\mathbf{x}}) = \mathbb{E}[(\hat{\mathbf{x}} - \mathbf{x})^T(\hat{\mathbf{x}} - \mathbf{x}); \mathbf{x}], \quad (17)$$

where $\mathbb{E}[\cdot; \mathbf{x}]$ denotes the expectation parametrized by the deterministic parameter vector, \mathbf{x} . The estimation error vector

of the GFR-ML estimator, $\hat{\mathbf{x}} - \mathbf{x}$, is obtained by substituting (9), (13), and (14), and using the identity

$$\mathbf{I} - (\mathbf{A} + \mathbf{B})^{-1}\mathbf{A} = (\mathbf{A} + \mathbf{B})^{-1}\mathbf{B}$$

with $\mathbf{A} = h_{\mathbf{M}}^T(\mathbf{L})\mathbf{D}\mathbf{R}^{-1}\mathbf{D}h_{\mathbf{M}}(\mathbf{L})$ and $\mathbf{B} = \mu h_{\mathbf{R}}^+(\mathbf{L})$, which results in

$$\hat{\mathbf{x}} - \mathbf{x} = \mathbf{K}^{-1}(\mathbf{d})(h_{\mathbf{M}}^T(\mathbf{L})\mathbf{D}\mathbf{R}^{-1}\mathbf{D}\mathbf{e} + h_{\mathbf{R}}^+(\mathbf{L})(\mathbf{x}_0 - \mathbf{x})). \quad (18)$$

By substituting (18) in (17) and using the fact that the covariance of $\mathbf{D}\mathbf{e}$ is $\mathbf{D}\mathbf{R}\mathbf{D}$, we obtain that the MSE of the GFR-ML estimator is

$$\begin{aligned} \mathbb{E}[(\hat{\mathbf{x}} - \mathbf{x})^T(\hat{\mathbf{x}} - \mathbf{x}); \mathbf{x}] &= \mu^2 \|\mathbf{K}^{-1}(\mathbf{d})h_{\mathbf{R}}^+(\mathbf{L})(\mathbf{x} - \mathbf{x}_0)\|^2 \\ &+ \text{tr}\left(\mathbf{K}^{-1}(\mathbf{d})h_{\mathbf{M}}^T(\mathbf{L})\mathbf{D}\mathbf{R}^{-1}\mathbf{D}h_{\mathbf{M}}(\mathbf{L})\mathbf{K}^{-1}(\mathbf{d})\right). \end{aligned} \quad (19)$$

The MSE of the GFR-ML estimator in (19) is a function of the unknown input graph signal, \mathbf{x} . Thus, it cannot be used as the cost function for the optimization of the sensor locations, $C(\mathbf{d})$. This dependency arises because there is no assumption about the prior distribution of \mathbf{x} , and the MSE cannot be averaged over it, which, in this case, results in a bias term that depends on \mathbf{x} . Moreover, since the input signal can vary across different network deployments or estimation tasks, optimizing sensor locations based directly on the MSE is impractical, as sensor deployment is typically conducted during the initial setup, and their locations cannot adapt dynamically to changes in the signal. Therefore, alternative cost functions must be considered that can approximate or bound the MSE without being a function of \mathbf{x} .

IV. PROPOSED SAMPLING ALLOCATION

In this section, we introduce four possible cost functions $C(\mathbf{d})$ for the sampling allocation scheme: the bCRB (Subsection IV-A), WC-MSE (Subsection IV-B), BMSE (Subsection IV-C), and WC-BMSE (Subsection IV-D). General remarks on the relations between these cost functions are provided in Subsection IV-E.

A. Cost Function 1: bCRB

The first cost function is based on replacing the MSE from (19) with the bCRB [50]. The bCRB provides a lower bound on the MSE for any estimator with a given bias function, under mild regularity conditions [50]. In our case, the distribution of the partial measurement vector obtained from the sensor subset \mathcal{S} , as described in (9), is as follows:

$$\mathbf{D}\mathbf{y} \sim \mathcal{N}(\mathbf{D}h_{\mathbf{M}}(\mathbf{L})\mathbf{x}, \mathbf{R}). \quad (20)$$

The bCRB on the trace of the MSE for this Gaussian model is given by (see, e.g. pp. 45-46 in [50])

$$\begin{aligned} \text{bCRB}(\mathbf{d}) &\triangleq \text{tr}\left((\mathbf{I} + \nabla_{\mathbf{x}}\mathbf{b}(\mathbf{x}, \mathbf{d})) \right. \\ &\quad \left. \times (h_{\mathbf{M}}^T(\mathbf{L})\mathbf{D}\mathbf{R}^{-1}\mathbf{D}h_{\mathbf{M}}(\mathbf{L}))^\dagger (\mathbf{I} + \nabla_{\mathbf{x}}\mathbf{b}(\mathbf{x}, \mathbf{d}))^T\right), \end{aligned} \quad (21)$$

where $\nabla_{\mathbf{x}}\mathbf{b}(\mathbf{x}, \mathbf{d}) \in \mathbb{R}^{N \times N}$ is the Jacobian matrix of the estimator bias, defined as $\mathbf{b}(\mathbf{x}, \mathbf{d}) \triangleq \mathbb{E}[\hat{\mathbf{x}} - \mathbf{x}]$. It should be noted that for $|\mathcal{S}| < N$, \mathbf{D} is not a full rank matrix. Consequently, the Fisher information matrix (FIM) is also not full rank, as it results from the multiplication of singular

matrices. Therefore, the use of the pseudo-inverse in (21) enables the the option of a singular FIM [51].

By using the model in (9) and the estimator in (13), we obtain that the bias of the GFR-ML estimator is

$$\mathbf{b}(\mathbf{x}, \mathbf{d}) = \mathbf{K}^{-1}(\mathbf{d})(h_M^T(\mathbf{L})\mathbf{D}\mathbf{R}^{-1}\mathbf{D}h_M(\mathbf{L})\mathbf{x} + \mu h_R^+(\mathbf{L})\mathbf{x}_0) - \mathbf{x}. \quad (22)$$

Thus, the gradient of the bias from (22) w.r.t. \mathbf{x} is

$$\nabla_{\mathbf{x}}\mathbf{b}(\mathbf{x}, \mathbf{d}) = \mathbf{K}^{-1}(\mathbf{d})h_M^T(\mathbf{L})\mathbf{D}\mathbf{R}^{-1}\mathbf{D}h_M(\mathbf{L}) - \mathbf{I}. \quad (23)$$

By substituting (23) in (21), and using the pseudo-inverse property $\mathbf{A} = \mathbf{A}\mathbf{A}^\dagger\mathbf{A}$, we obtain that the bCRB on the MSE of estimators with the GFR-ML bias is given by

$$\text{bCRB}(\mathbf{d}) = \text{tr}\left(\mathbf{K}^{-1}(\mathbf{d})h_M^T(\mathbf{L})\mathbf{D}\mathbf{R}^{-1}\mathbf{D}h_M(\mathbf{L})\mathbf{K}^{-1}(\mathbf{d})\right). \quad (24)$$

It can be seen that for the special case of $\mathbf{x} = \mathbf{x}_0$, the MSE of the GFR-ML estimator from (19) coincides with the bCRB given in (24). For the special case that $h_M(\mathbf{L}) = \mathbf{L}$ and $h_R(\mathbf{L}) = \mathbf{L}$ in (24), the sampling scheme from our previous work [5] is obtained.

B. Cost Function 2: WC-MSE

As an alternative way to address the dependency of the MSE in (19) of the unknown parameter \mathbf{x} , we describe here a cost function that is based on a worst-case bias at \mathbf{x} in the neighborhood of \mathbf{x}_0 , similar to the rationale in [52]. Specifically, we tested values of \mathbf{x} that lie in the unit ball centered at \mathbf{x}_0 , $\mathcal{B}(\mathbf{x}_0) \triangleq \{\forall \mathbf{x} \in \mathbb{R}^N \mid \|\mathbf{x} - \mathbf{x}_0\| \leq 1\}$, and define the associated WC-MSE of $\hat{\mathbf{x}}$ as

$$\begin{aligned} \text{MSE}_{WC}(\mathbf{d}) &\triangleq \max_{\mathbf{x} \in \mathcal{B}(\mathbf{x}_0)} \mathbb{E}[(\hat{\mathbf{x}} - \mathbf{x})^T(\hat{\mathbf{x}} - \mathbf{x})] \\ &= \text{bCRB}(\mathbf{d}) + \max_{\mathbf{x} \in \mathcal{B}(\mathbf{x}_0)} \mu^2 \|\mathbf{K}^{-1}(\mathbf{d})h_R^+(\mathbf{L})(\mathbf{x} - \mathbf{x}_0)\|^2 \\ &= \text{bCRB}(\mathbf{d}) + \mu^2 \lambda_{\max}\left(h_R^+(\mathbf{L})\mathbf{K}^{-2}(\mathbf{d})h_R^+(\mathbf{L})\right), \end{aligned} \quad (25)$$

where the second equality is obtained by substituting (19) and (24), and the third equality is obtained by using the Rayleigh quotient theorem ([53], pp. 234-235). It can be seen that the first term in (25) captures the contribution of the measurement noise, while the second term, which is the spectral norm of $h_R^+(\mathbf{L})\mathbf{K}^{-2}(\mathbf{d}, \mu)h_R^+(\mathbf{L})$ ([53], p. 346), quantifies the worst-case impact of the regularization via its spectral norm. The WC-MSE provides a robust metric for reliable estimation under unfavorable conditions. The constraint $\mathbf{x} \in \mathcal{B}(\mathbf{x}_0)$ normalizes deviations from the reference signal \mathbf{x}_0 , focusing on worst-case directional impacts while preventing unbounded estimation error. When \mathbf{x}_0 is a reliable prior, the constraint captures signal deviations within a specific range, modeling uncertainty while keeping the problem tractable.

C. Cost Function 3: BMSE

Until this subsection, the variable \mathbf{x} has been treated as deterministic. In this subsection, we adopt a Bayesian perspective, as described in (11), where $\mathbf{x} \sim \mathcal{N}(\mathbf{x}_0, \frac{1}{\mu}(f^2(\mathbf{A}))^\dagger)$. Then, we derive the theoretical minimum MSE for the Bayesian setting. The Bayesian trace MSE of the MMSE estimator, $\mathbb{E}[\mathbf{x}|\mathbf{y}]$, is given by (see p. 347 [50])

$$\text{BMSE}(\mathbf{d}) = \mathbb{E}[\mathbb{E}[(\mathbb{E}[\mathbf{x}|\mathbf{y}] - \mathbf{x})^T(\mathbb{E}[\mathbf{x}|\mathbf{y}] - \mathbf{x})|\mathbf{x}]], \quad (26)$$

where we used the Law of Total Expectation.

As discussed in Subsection III-B (after (11)), the GFR-ML estimator from (13)-(14) is equivalent to the MMSE estimator in the Bayesian setting, i.e. $\mathbb{E}[\mathbf{x}|\mathbf{y}] = \hat{\mathbf{x}}$, where $\hat{\mathbf{x}}$ is defined in (13) and \mathbf{x} is treated as a random variable in (26). Thus, the inner (conditional) expectation in (26) coincides with the non-Bayesian MSE expression derived in (19), with \mathbf{x} now treated as random. By substituting (19) in (26) and calculating the expectation w.r.t. \mathbf{x} , one obtains

$$\begin{aligned} \text{BMSE}(\mathbf{d}) &= \mathbb{E}_{\mathbf{x}}\left[\text{tr}\left(\mathbf{K}^{-2}(\mathbf{d})h_M^T(\mathbf{L})\mathbf{D}\mathbf{R}^{-1}\mathbf{D}h_M(\mathbf{L})\right)\right] \\ &\quad + \mu^2 \text{tr}\left(\mathbb{E}[(\mathbf{x}_0 - \mathbf{x})(\mathbf{x}_0 - \mathbf{x})^T]h_R^+(\mathbf{L})\mathbf{K}^{-2}(\mathbf{d})h_R^+(\mathbf{L})\right), \end{aligned} \quad (27)$$

where we used the trace operator definition and its property $\text{tr}(\mathbf{A}\mathbf{B}) = \text{tr}(\mathbf{B}\mathbf{A})$. By changing the order of the trace and the expectation operators, substituting $\mathbb{E}[(\mathbf{x} - \mathbf{x}_0)(\mathbf{x} - \mathbf{x}_0)^T] = \frac{1}{\mu}(h_R^+(\mathbf{L}))^\dagger$ (according to (11)) in (27), and applying the pseudo-inverse property $\mathbf{A} = \mathbf{A}\mathbf{A}^\dagger\mathbf{A}$, we simplify (27) as follows:

$$\begin{aligned} \text{BMSE}(\mathbf{d}) &= \text{tr}\left(\mathbf{K}^{-2}(\mathbf{d})(h_M^T(\mathbf{L})\mathbf{D}\mathbf{R}^{-1}\mathbf{D}h_M(\mathbf{L}) + \mu h_R^+(\mathbf{L}))\right) \\ &= \text{tr}(\mathbf{K}^{-1}(\mathbf{d})), \end{aligned} \quad (28)$$

where the last equality is obtained by substituting the definition of $\mathbf{K}(\mathbf{d})$ from (14). The BMSE in (28) coincides with the Bayesian CRB in this case. The Bayesian CRB is attainable by the MMSE here, since the posterior distribution of \mathbf{x} is Gaussian. Consequently, the cost function in (28) can also be interpreted as a Bayesian CRB cost function [32].

D. Cost Function 4: WC-BMSE

Instead of taking the trace of the BMSE matrix (i.e. its Frobenius norm [53], pp. 341-342) as in (28), we here consider the spectral norm ([53], p. 346) of the MSE matrix:

$$\text{BMSE}_{wc}(\mathbf{d}) = \lambda_{\max}\left(\mathbf{K}^{-1}(\mathbf{d})\right) = \lambda_{\min}^{-1}\left(\mathbf{K}(\mathbf{d})\right), \quad (29)$$

where the last equality follows from Theorem 4.2.2 in [53].

It is important to note that if $\mathbf{K}(\mathbf{d})$ is not invertible for some \mathbf{d} , the inverse is replaced by the pseudo-inverse. Consequently, the second equality holds for the minimal eigenvalue that is nonzero. The reformulation on the right-hand side of (29), eliminates the need to invert $\mathbf{K}(\mathbf{d})$, and is therefore more computationally efficient.

Claim 1. *The cost function in (29) can be interpreted as the WC-BMSE in the Bayesian approach, measured in the Mahalanobis distance sense.*

Proof. In this claim, we use the Mahalanobis distance to measure the distance between $\mathbf{z} \triangleq [\mathbf{e}^T, \mathbf{x}^T]^T$ and its distribution. First, it can be seen that $\mathbf{z} \sim \mathcal{N}(\bar{\mathbf{z}}, \mathbf{R}_{\mathbf{z}})$, where $\bar{\mathbf{z}} \triangleq [\mathbf{0}^T, \mathbf{x}_0^T]^T$ and $\mathbf{R}_{\mathbf{z}} \triangleq \begin{pmatrix} \mathbf{R} & \mathbf{0} \\ \mathbf{0} & (h_R^+(\mathbf{L}))^\dagger \end{pmatrix}$. The Mahalanobis distance constraint can then be expressed as follows:

$$\|\mathbf{z} - \bar{\mathbf{z}}\|_{\mathbf{R}_{\mathbf{z}}^\dagger} \leq 1, \quad (30)$$

which restricts the vector \mathbf{z} to lie within an ellipsoid determined by its prior distribution. Then, it can be verified

that by substituting the GFR-ML estimator form from (13)-(14), the WC-BMSE of an estimator $\hat{\mathbf{x}}$ satisfies

$$\begin{aligned} & \max_{\|\mathbf{z}-\bar{\mathbf{z}}\|_{\mathbf{R}_z^{-1}} \leq 1} \|\mathbf{x} - \hat{\mathbf{x}}\|^2 \\ &= \max_{\|\mathbf{z}-\bar{\mathbf{z}}\|_{\mathbf{R}_z^{-1}} \leq 1} \|\mathbf{K}^{-1}(\mathbf{d})\mathbf{H}\mathbf{R}_z^\dagger(\mathbf{z} - \bar{\mathbf{z}})\|^2, \end{aligned} \quad (31)$$

where $\mathbf{H} \triangleq (h_M(\mathbf{L}), \mathbf{I})^T$. Using the Rayleigh-Ritz Theorem for the vector $(\mathbf{R}_z^{1/2})^\dagger(\mathbf{z} - \bar{\mathbf{z}})$, the solution to (31) is expressed as

$$\lambda_{\max}((\mathbf{R}_z^{1/2})^\dagger \mathbf{H}^T \mathbf{K}^{-2}(\mathbf{d}) \mathbf{H} (\mathbf{R}_z^{1/2})^\dagger) = \lambda_{\max}(\mathbf{K}^{-1}(\mathbf{d})), \quad (32)$$

where we substituted $\mathbf{K}(\mathbf{d})$ from (14) and used the property $\lambda_i(\mathbf{A}\mathbf{A}^T) = \lambda_i^2(\mathbf{A}^T\mathbf{A})$ with $\mathbf{A} = \mathbf{K}^{-1}(\mathbf{d}, \mu)\mathbf{H}(\mathbf{R}_z^{1/2})^\dagger$. It can be seen that the last term in (32) coincides with $\text{BMSE}_{wc}(\mathbf{d})$, which completes the proof. \square

E. Discussion and General Remarks

The cost functions in (24), (25), (28), and (29) are not a function of the unknown input graph signal, \mathbf{x} . This property enables their practical use for choosing the sampling set or sensor locations by replacing $C(\mathbf{d})$ in (15) with any of these cost functions. These cost functions can also be utilized for general system design, such as selecting the optimal graph filter for regularization to improve estimation performance. In the following we discuss some properties and special cases of the proposed approach.

1) *Full observability without regularization*: If all sensors are available and no regularization is applied, then, substituting $\mathbf{d} = \mathbf{1}$ and $\mu = 0$ in (14) yields:

$$\mathbf{K}(\mathbf{d} = \mathbf{1}, \mu = 0) = h_M^T(\mathbf{L})\mathbf{R}^{-1}h_M(\mathbf{L}). \quad (33)$$

Substituting (33) into any of the proposed cost functions, (24), (25), (28), and (29), results in

$$C(\hat{\mathbf{x}}, \mathbf{d} = \mathbf{1}) = \text{tr}((h_M^T(\mathbf{L})\mathbf{R}^{-1}h_M(\mathbf{L}))^\dagger). \quad (34)$$

The equivalence of the proposed cost functions in this extreme case provides additional justification for their use. Moreover, by using (22), it can be seen that in this case the bias is $\mathbf{b}(\mathbf{d}) = \mathbf{0}$. Thus, the unbiased CRB, which can be obtained from (24) with zero bias, reduces to the expression in (34).

2) *Large μ* : For simplicity in the following analysis, we assume that $h_R^+(\mathbf{L})$ is full column rank. Then, for $\mu \rightarrow \infty$, the following asymptotic properties hold:

$$\lim_{\mu \rightarrow \infty} \mathbf{K}^{-1}(\mathbf{d}, \mu) = \mathbf{0}, \quad (35)$$

$$\lim_{\mu \rightarrow \infty} \mu^2 h_R^+(\mathbf{L})\mathbf{K}^{-2}(\mathbf{d}, \mu)h_R^+(\mathbf{L}) = \mathbf{I}. \quad (36)$$

Thus, for $\mu \rightarrow \infty$, from (36) and (13) $\hat{\mathbf{x}} = \mathbf{x}_0$, i.e. the estimator ignores the measurements and uses only the prior mean, \mathbf{x}_0 .

Since the sensor data is not informative in this case, the cost functions become degenerative, as described in the following. By substituting (36) in (19), we obtain that the non-Bayesian MSE satisfies

$$\lim_{\mu \rightarrow \infty} \text{MSE}(\mathbf{d}) = \|\mathbf{x}_0 - \mathbf{x}\|_2^2. \quad (37)$$

By substituting (35) in (24), we obtain that the bCRB approaches zero as $\mu \rightarrow \infty$: $\lim_{\mu \rightarrow \infty} \text{bCRB}(\mathbf{d}) = \mathbf{0}$.

Similarly, by substituting (36) in (25), it can be seen that for $\mu \rightarrow \infty$, the WC-MSE converges to 1, since

$$\begin{aligned} \lim_{\mu \rightarrow \infty} \max_{\mathbf{x}: \|\mathbf{x} - \mathbf{x}_0\|_2 = 1} \text{MSE}(\mathbf{d}) &= \max_{\mathbf{x}: \|\mathbf{x} - \mathbf{x}_0\|_2 = 1} \lim_{\mu \rightarrow \infty} \text{MSE}(\mathbf{d}) \\ &= \max_{\mathbf{x}: \|\mathbf{x} - \mathbf{x}_0\|_2 = 1} \|\mathbf{x} - \mathbf{x}_0\|_2^2, \end{aligned} \quad (38)$$

where the last equality is obtained by substituting (37).

The BMSE (28) and the WC-BMSE (29) approach zero because, from a Bayesian perspective, $\mathbf{x} \sim \mathcal{N}(\mathbf{x}_0, \frac{1}{\mu}(h_R^+(\mathbf{L}))^\dagger)$. As $\mu \rightarrow \infty$, this implies that \mathbf{x} becomes a deterministic parameter equal to the mean, and, therefore, the deviation from the prior is zero.

Thus, we can conclude that under all cost functions, taking an excessively large value of μ disregards the observation. This emphasizes the importance of appropriately tuning μ to balance prior information and observed data.

3) *Relation with the Laplacian-regularized design*: In [30], the following sampling allocation was proposed:

$$\mathbf{d}^{LR} = \arg \max_{\mathbf{d} \in \{0,1\}^N: \|\mathbf{d}\|_2 = q} \lambda_{\min}(\mathbf{D}^T\mathbf{D} + \mu\mathbf{L}). \quad (39)$$

It can be seen that if $h_M(\mathbf{L}) = \mathbf{I}$, $\mathbf{R} = \mathbf{I}$, $h_R^+(\mathbf{L}) = \mathbf{L}$, and $\mathbf{x}_0 = \mathbf{0}$, the WC-BMSE cost function from (29) coincides with the Laplacian-regularized sampling. The proposed WC-BMSE cost function in this work can be seen as a generalization to different choices of $h_M(\mathbf{L})$, $h_R^+(\mathbf{L})$, \mathbf{x}_0 , and \mathbf{R} .

4) *Relationship with the bandlimitedness approaches*: The widely used GSP criteria for sampling and recovery are based on graph bandlimitedness assumptions, and aim to minimize different forms of the MSE of constrained bandlimited estimators. In particular, the most commonly used sampling schemes in GSP are the A-design [14] and E-design [16] approaches, given by

$$\mathbf{d}^{A\text{-design}} = \arg \min_{\mathbf{d} \in \{0,1\}^N: \|\mathbf{d}\|_2 = q} \text{tr}((\mathbf{V}_{S,\mathcal{R}}^T \mathbf{V}_{S,\mathcal{R}})^{-1}), \quad (40)$$

$$\mathbf{d}^{E\text{-design}} = \arg \max_{\mathbf{d} \in \{0,1\}^N: \|\mathbf{d}\|_2 = q} \lambda_{\min}(\mathbf{V}_{S,\mathcal{R}}^T \mathbf{V}_{S,\mathcal{R}}), \quad (41)$$

where $\mathcal{R} \subseteq \mathcal{V}$ is the subset of frequency indices associated with the bandlimited graph signal.

The following claim states that for the special case where the measurement model captures a bandlimited graph signal over the frequency set \mathcal{R} and the regularization strongly suppresses frequency components in the rest of the spectrum, $\mathcal{S} \setminus \mathcal{R}$, the proposed Bayesian criteria align with the A-design and E-design cost functions. Therefore, the proposed Bayesian methods can be interpreted as generalizations of the A-design and E-design criteria for general graph filters.

Claim 2. *For the special case of recovering bandlimited graph signals, i.e. where*

$$\begin{aligned} h_M(\mathbf{L}) &= \mathbf{V} \text{diag}(\mathbf{1}_{\{\mathcal{R}\}}) \mathbf{V}^{-1}, \quad \mathbf{x}_0 = \mathbf{0}, \quad \text{and} \\ (h_R^+(\mathbf{L}))^\dagger &= \mathbf{V} \text{diag}(\mu \mathbf{1}_{\{\mathcal{S} \setminus \mathcal{R}\}}) \mathbf{V}^{-1}, \end{aligned} \quad (42)$$

with $\mathbf{R} = \mathbf{I}$, the BMSE from (28) coincides with the A-design cost from (40). If, additionally, $\mu \geq \lambda_{\min}(\mathbf{V}_{S,\mathcal{R}}^T \mathbf{V}_{S,\mathcal{R}})$, the WC-BMSE from (29) coincides with the E-design cost function from (41).

Proof. The proof appears in Appendix A. \square

V. SENSOR SELECTION SOLVERS

Finding the set of $q < N$ sensor locations from the N nodes to minimize the different cost functions, as described in (15), is a combinatorial optimization problem that has, in the worst case, a computational complexity of $\binom{N}{q}$, which is computationally prohibitive for large-scale systems. Thus, we propose two iterative approaches as follows. In Subsection V-A, we present a heuristic method that iteratively selects sensor locations in order to approximate the solution of (15). In Subsection V-B we derive a PGD method to solve a relaxation of (15), providing a computationally efficient solution with a complexity reduction by a factor of approximately N .

A. Greedy Algorithm

In this subsection, we introduce a greedy algorithm, described in Algorithm 1, for the practical implementation of the sensor selection problem. While greedy algorithms do not guarantee optimality, they often perform well in practice. The core idea behind this algorithm is to iteratively add to the sampling set those nodes that minimize the chosen cost function. The stopping criterion depends on the chosen optimization: either selecting a fixed number of sensors q (as stated in (15)) or achieving a predefined error threshold (as stated in (16)).

Algorithm 1 Greedy Selection of the Measured Nodes

Input: graph filters, $h_{\mathbf{R}}^+(\mathbf{L})$, $h_{\mathbf{M}}(\mathbf{L})$, number of nodes, q , noise covariance matrix, \mathbf{R} , and regularization parameter, μ

Initialization: Set the initial sampling subset $\mathcal{S}^{(0)} = \emptyset$ and the iteration index, $i = 0$

while $i < q$

- 1) Update the set of available nodes: $\mathcal{L} = \mathcal{V} \setminus \mathcal{S}^{(i)}$
- 2) Select the node that minimizes the cost function:

$$w^{opt} = \arg \min_{w \in \mathcal{L}} C(\mathbf{1}_{\{\mathcal{S}^{(i)} \cup w\}}) \quad (43)$$

where $C(\mathbf{d})$ is one of the proposed cost functions defined in (24), (25), (28), or (29).

- 3) Update the sampling set: $\mathcal{S}^{(i+1)} \leftarrow \mathcal{S}^{(i)} \cup w^{opt}$, and increment the iteration index, $i \leftarrow i + 1$

Output: Subset of the selected q nodes: $\mathcal{S} = \mathcal{S}^{(i)}$

The computational complexity of Algorithm 1 depends on the complexity of evaluating the cost function $C(\mathbf{d})$ for each set of sensors (i.e. in each iteration, in (43)) and on the desired number of sensors, q . Since a single calculation of $C(\mathbf{d})$ from (21), (25), and (28) has a computational complexity of $O(N^3)$ (the computational complexity of (29) is $O(N^2)$ [54]), this method requires $\sum_{n=0}^{q-1} (N - n)$ calculations of $C(\mathbf{d})$ without any search-reduction rules (i.e. N options for the first node, $N - 1$ options for the second node, and so on). This summation results in $q(N - \frac{q-1}{2})$ calculations. The total complexity becomes $O(q(N - \frac{q-1}{2})N^3)$ (or $O(q(N - \frac{q-1}{2})N^2)$ for (29)), which is computationally prohibitive for a large N . Consequently, while the greedy approach is straightforward, its high computational cost for large graphs necessitates the development of more efficient methods. In the following subsection, we propose a more efficient PGD algorithm.

B. Alternating PGD

A common approach for dealing with binary decision variables, such as \mathbf{d} , is to relax them to continuous variables,

and subsequently, to project the solution onto the feasible set of the original problem [31]. To simplify the problem in (15), we relax the non-convex Boolean constraint $\mathbf{d} \in \{0, 1\}^N$ to the convex box constraint $\mathbf{d} \in [0, 1]^N$, and the norm constraint to a ball constraint, i.e. $\|\mathbf{d}\|_2^2 = q$ to $\|\mathbf{d}\|_2^2 \leq q$. The relaxed optimization problem is then formulated as follows:

$$\begin{aligned} \hat{\mathbf{d}} &= \arg \min_{\mathbf{d} \in \mathbb{R}^N} C(\mathbf{d}) \\ \text{s.t. } & \|\mathbf{d}\|_2^2 \leq q, \\ & 0 \leq d_n \leq 1, \quad n = 1, 2, \dots, N. \end{aligned} \quad (44)$$

To implement this approach, we derive the associated PGD algorithm (see p. 223 in [55]), which iteratively combines a gradient descent step and a projection step. First, a gradient descent step with a backtracking linesearch [56] is performed to determine a step size ρ that reduces the cost function as follows. We start from an initial value, ρ , which is iteratively reduced until the following condition no longer holds:

$$C(\mathcal{P}(\mathbf{d}^{(k)} - \rho \nabla C(\mathbf{d}^{(k)}))) > C(\mathcal{P}(\mathbf{d}^{(k)})), \quad (45)$$

where $\nabla C(\mathbf{d}^{(k)})$ is the gradient of the cost function w.r.t. \mathbf{d} evaluated at $\mathbf{d}^{(k)}$, and \mathcal{P} denotes the projection operator onto the feasible set of the original problem,

$$\mathcal{P}(\mathbf{y}) \triangleq \mathcal{P}_{\{\mathbf{d} \in \{0, 1\}^N \mid \|\mathbf{d}\|_2^2 \leq q\}}(\mathbf{y}). \quad (46)$$

Once the step size ρ is determined, the vector is updated as:

$$\mathbf{d}^{(k+1)} = \mathbf{d}^{(k)} - \rho \nabla C(\mathbf{d}^{(k)}), \quad (47)$$

where the update skips projection onto the non-convex binary set to avoid zero-gradient points in subsequent iterations.

Next, we perform a projection of the result onto the constrained set of the relaxed problem from (44), which in our case is given by

$$\mathbf{d}^{(k+1)} \leftarrow \mathcal{P}_{\{\mathbf{d} \in \mathbb{R}^N \mid \|\mathbf{d}\|_2^2 \leq q, \mathbf{0} \leq \mathbf{d} \leq \mathbf{1}\}}(\mathbf{d}^{(k+1)}). \quad (48)$$

The set $\{\mathbf{d} \in \mathbb{R}^N \mid \|\mathbf{d}\|_2^2 \leq q, \mathbf{0} \leq \mathbf{d} \leq \mathbf{1}\}$ is the intersection of two convex sets. Thus, the projection step can be simplified by using alternating PGD [57], where the projection alternates sequentially between the two sets as follows:

- 1) Projection onto the ℓ_2 -norm constraint:

$$\mathcal{P}_{\{\mathbf{d} \in \mathbb{R}^N \mid \|\mathbf{d}\|_2^2 \leq q\}}(\mathbf{y}) = \begin{cases} \frac{q}{\|\mathbf{y}\|_2^2} \mathbf{y} & , \quad \|\mathbf{y}\|_2^2 \geq q \\ \mathbf{y} & , \quad \text{otherwise} \end{cases}. \quad (49)$$

This projection corresponds to the solution of Problem 4.22, p. 197 in [56].

- 2) Projection onto the box constraint:

$$\mathcal{P}_{\{\mathbf{d} \in \mathbb{R}^N \mid \mathbf{0} \leq \mathbf{d} \leq \mathbf{1}\}}(\mathbf{y}) = \max\{\min\{\mathbf{y}, \mathbf{1}\}, \mathbf{0}\}, \quad (50)$$

$\forall \mathbf{y} \in \mathbb{R}^N$. This projection is obtained by the solution to the well-known Euclidean projection onto a rectangle (see, e.g. p. 399 in [56]).

The PGD algorithm is summarized in Algorithm 2.

Algorithm 2 uses the gradient of the cost function in Step 1), where the gradients of the considered cost functions are provided in the following claim.

Claim 3. *The gradient of the cost functions from (24), (25), (28), and (29) w.r.t. \mathbf{d} can be written as*

Algorithm 2 Alternating Projected Gradient Descent for (44)

Input: $\mathbf{d}^{(0)}$, cost function $C(\mathbf{d})$, initial step size ρ_0 , linesearch backtracking parameter $0 < \beta < 1$, maximum number of PGD iterations M_1 , and tolerance ε

Initialization: $\rho = \rho_0$

for $k = 0, \dots, M_1$

- 1) **{while** condition (45) satisfied **do:** $\rho \leftarrow \beta\rho$
Update solution

$$\mathbf{d}^{(k+1)} \leftarrow \mathbf{d}^{(k)} - \rho \nabla C(\mathbf{d}^{(k)}) \quad (\text{see (47)})$$

- 2) Project onto the ℓ_2 -norm constraint set:

$$\mathbf{d}^{(k+1)} \leftarrow \frac{q}{\|\mathbf{d}^{(k+1)}\|_2^2} \mathbf{d}^{(k+1)} \quad (\text{see (49)}).$$

- 3) Project onto the box constraint:

$$\mathbf{d}^{(k+1)} \leftarrow \max\{\min\{\mathbf{d}^{(k+1)}, \mathbf{1}\}, \mathbf{0}\} \quad (\text{see (50)})$$

- 4) $k \leftarrow k + 1$, and $\rho \leftarrow \rho_0$

- 5) **if** $\|\mathbf{d}^{(k)} - \mathbf{d}^{(k-1)}\|_2 \leq \varepsilon$ **break**

Output: Final solution in the constrained set, $\mathcal{P}(\mathbf{d}^{(k)})$

$$\nabla C(\mathbf{d}) = -2\text{diag}(\mathbf{R}^{-1}\mathbf{D}h_{\mathbf{M}}(\mathbf{L})\mathbf{K}^{-1}(\mathbf{d})\mathbf{Q}\mathbf{K}^{-1}(\mathbf{d})h_{\mathbf{M}}(\mathbf{L})), \quad (51)$$

where the matrix \mathbf{Q} for each cost function is

$$\mathbf{Q}_{\text{bCRB}} = \mathbf{I} - \mathbf{K}^{-1}(\mathbf{d})h_{\mathbf{R}}^+(\mathbf{L}) - h_{\mathbf{R}}^+(\mathbf{L})\mathbf{K}^{-1}(\mathbf{d}), \quad (52)$$

$$\mathbf{Q}_{\text{MSE-wc}} = \left(\mathbf{I} - \mathbf{K}^{-1}(\mathbf{d})h_{\mathbf{R}}^+(\mathbf{L})(\mathbf{I} - \mathbf{u}_{\max}\mathbf{u}_{\max}^T h_{\mathbf{R}}^+(\mathbf{L})) \right. \\ \left. - (\mathbf{I} - h_{\mathbf{R}}^+(\mathbf{L})\mathbf{u}_{\max}\mathbf{u}_{\max}^T)h_{\mathbf{R}}^+(\mathbf{L})\mathbf{K}^{-1}(\mathbf{d}) \right), \quad (53)$$

$$\mathbf{Q}_{\text{BMSE}} = \mathbf{I}, \quad (54)$$

$$\mathbf{Q}_{\text{BMSE-wc}} = \lambda_{\min}^{-2}(\mathbf{K}(\mathbf{d}))\mathbf{K}(\mathbf{d})\mathbf{u}_{\min}\mathbf{u}_{\min}^T\mathbf{K}(\mathbf{d}), \quad (55)$$

and in (53) \mathbf{u}_{\max} is the normalized eigenvector corresponding to $\lambda_{\max}(h_{\mathbf{R}}^+(\mathbf{L})\mathbf{K}^{-2}(\mathbf{d})h_{\mathbf{R}}^+(\mathbf{L}))$, and in (55) \mathbf{u}_{\min} is the normalized eigenvector corresponding to $\lambda_{\min}(\mathbf{K}(\mathbf{d}))$.

Proof. The derivations of (51)-(55) appear in Appendix B. \square

Initialization of Algorithm 2 - It can be seen that if $\mathbf{R} = \sigma^2\mathbf{I}$, $\sigma \in \mathbb{R}$, (52)-(55) imply that the n th entry of the gradient of $C(\mathbf{d})$ is zero for $d_n = 0$. Consequently, if the initial guess is set to $d_n^{(0)} = 0$, the n th entry remains fixed at zero throughout the optimization process, which may prevent the algorithm from finding a solution that minimizes the cost function. To mitigate this issue, we suggest initializing \mathbf{d} as an arbitrary feasible solution such that $\mathbf{d} \in (0, 1)^N$, for any \mathbf{R} . This approach reduces the dependence of the output on the initial guess.

The **computational complexity of Algorithm 2** is based on calculating each of the cost functions in (24), (25), (28), as well as their gradients in (52)-(54), which is $O(N^3)$ (the computational complexity of (29) as well as its gradient (55) is $O(N^2)$ [54]). Let M_1 denote the number of PGD iterations required for convergence and M_2 denote the maximum number of backtracking linesearch iterations needed to evaluate the cost function per iteration. Consequently, the total worst-case complexity of the algorithm is $O(M_1M_2N^3)$ (or $O(M_1M_2N^2)$ for the WC-BMSE), but the computational burden is often significantly lower. Typically, several dozen

iterations M_1 are required to guarantee convergence, and the first linesearch attempt is often successful, reducing the effective complexity to approximately $O(M_1N^3)$ (or $O(M_1N^2)$ for the WC-BMSE). This makes the proposed PGD method significantly faster than the greedy algorithm, which has a complexity of $O(q(N - \frac{q-1}{2})N^3)$ (or $O(q(N - \frac{q-1}{2})N^2)$ for the WC-BMSE), and can approach $O(N^5)$ ($O(N^4)$) when q is proportional to N .

VI. SIMULATIONS

In this section, we compare the performance of the GFR-ML from (13)-(14) for synthetic data (Subsection VI-A), electrical networks data (Subsection VI-B), and road network data (Subsection VI-C) using the following sampling policies:

- (i) A-design [14]—the method presented in (40),
- (ii) E-design [16]—the method presented in (41),
- (iii) LR-design [30]—the method presented in (39),
- (iv) bCRB—the method presented in (15) with the cost function from (24),
- (v) WC-MSE—the method presented in (15) with the cost function from (25),
- (vi) BMSE—the method presented in (15) with the cost function from (28),
- (vii) WC-BMSE—the method presented in (15) with the cost function from (29).

Unless otherwise stated, we set $\mathcal{R} = 1, \dots, N/2$ for both the A-design and the E-design. The cost functions in i)-vii) lead to combinatorial problems, and, thus, are implemented here by Algorithm 1, and in Subsection VI-C by Algorithm 2, with the corresponding cost function as $C(\mathbf{d})$. In all simulations, the performance is evaluated using 10,000 Monte-Carlo simulations. Unless otherwise is stated, \mathbf{x} is generated by using (11), and \mathbf{y} is generated by substituting \mathbf{x} in the measurement model in (9), with $\mathbf{e} \sim \mathcal{N}(\mathbf{0}, 0.01\mathbf{I})$ and $\mu = 0.1$. This Bayesian setting is used to provide a comprehensive evaluation of the methods' performance, while avoiding reference to single-value results, as in a non-Bayesian setting.

A. Synthetic Data

In this subsection, we conduct simulations on an Erdős-Rényi graph model with 50 nodes, where each edge is included independently with a probability of 0.1. The edge weights of the graph are randomly drawn as $W_{k,n} \sim \mathcal{N}(5, 1), \forall (k, n) \in \xi$.

Figures 1.a-1.c present the MSE versus the percentage of sampled nodes, $\tilde{q} \triangleq q/N\%$, sampled according to the different methods, where the graph filters that were used to generate \mathbf{x} and \mathbf{y} according to the model in (9) and (11) appear in Table I, and are defined as follows:

- 1) Gaussian Markov random field (GMRF) with a Laplacian precision matrix [40], [46]: $h_{\text{GMRF}}(\lambda) = \frac{1}{\sqrt{\lambda}}$ for $\lambda \neq 0$ and zero otherwise,
- 2) Laplacian (Tikhonov) regularization [40], [58], [59]:

$$h_{\text{Tikh}}(\lambda) = \frac{1}{1 + \alpha\lambda}, \quad \alpha > 0, \quad (56)$$

- 3) Heat diffusion kernel [40], [60]:

$$h_{\text{Diff}}(\lambda) = \exp(-\tau\lambda), \quad \tau > 0. \quad (57)$$

Figure	1.a	1.b	1.c
$h_M(\mathbf{L})$	$(h_{\text{GMRF}}^2)^\dagger$	\mathbf{I}	$h_{\text{Diff}}^{-1}, \tau = 0.5$
$(h_R^+(\mathbf{L}))^\dagger$	h_{GMRF}^2	$h_{\text{Fikh}}^2, \alpha = 0.2$	\mathbf{I}

TABLE I: Graph filters that were used to create the data.

In Figs. 1.a-1.c the MSE decreases as the number of sampled nodes, \tilde{q} , increases, as expected, since there is more information for the estimate approach. In Fig. 1.a, we consider a realistic scenario where the estimated graph signal is smooth, but the measured graph signal is not (see, e.g. the power system example in Subsection VI-B). It can be seen that the estimation performance of the sampling sets selected by the BMSE and the WC-BMSE criteria outperform other sampling methods for any \tilde{q} . This is because methods such as A-design, E-design, and LR-design are based on the assumption that the measured signal is smooth/bandlimited, which does not hold here. In addition, the WC-MSE, which combines the bCRB and the worst-case bias (see in (25)), achieves significantly better recovery performance for $\tilde{q} > 60\%$ compared to the bCRB alone, highlighting the importance of accounting for bias.

In Fig. 1.b, we consider the case where both \mathbf{x} and \mathbf{y} are smooth. Here, the BMSE- and WC-BMSE-based estimations outperform the estimations based on the A-design, E-design, and LR-design. Although the data is smooth it is not strictly bandlimited, as these methods assume or have mismatches in graph filters (e.g. the LR-design assumes different $h_M(\mathbf{L})$ and $h_R^+(\mathbf{L})$ in (9) and (10) from the one used to generate the data). Furthermore, the bCRB and WC-MSE perform poorly on average, as they optimize locally for specific values of \mathbf{x} (bCRB assumes $\mathbf{x} = \mathbf{0}$, while WC-MSE assumes \mathbf{x} aligns with the largest eigenvector of the bias term in (19)).

In Fig. 1.c, we consider the test case of an inverse diffusion (high-pass filtering) process, i.e. $h_M(\mathbf{L}) = h_{\text{Diff}}^{-1}$, which can model the observation of anomalies or source localization in applications such as epidemic spreading or seismic activity [3], [11], [61], [62]. Here, we generate \mathbf{x} using all-pass graph filtering $h_R^+(\mathbf{L}) = \mathbf{I}$, which, when substituted into (10), results in the commonly used ℓ_2 regularization. Here, we set $\mathcal{R} = N/2, \dots, N$ in (40) and (41), as the measured signal passes through a graph HPF. The estimation based on WC-MSE, and WC-BMSE outperform all other methods for $\tilde{q} \leq 80\%$, as their conservative worst-case approach is well-suited to the highly varied data with high-frequency components resulting from the combination of all-pass and high-pass filtering. In contrast, the A-design, E-design, LR-design, bCRB, and BMSE exhibit suboptimal performance due to their model mismatches. Specifically, the A-design and E-design assume the graph filters from (42), the LR-design assumes $h_R^+(\mathbf{L}) = \mathbf{L}$, the bCRB assumes $\mathbf{x} = \mathbf{0}$, and the BMSE, which averages over all the eigenvalues of the Bayesian matrix in (28), is more sensitive to outliers from very high graph frequencies.

B. Power System Data

In order to demonstrate the practical application of our approach, we now present sensor allocation for power system state estimation (PSSE), which is at the core of energy management systems for various monitoring and analysis purposes. A power system can be represented as an undirected weighted graph, $\mathcal{G}(\mathcal{V}, \xi)$, where the node set \mathcal{V} comprises

the buses (generators or loads) and ξ is the set of edges that denote transmission lines [9], [63], [64]. The Laplacian matrix, \mathbf{L} , is constructed by using the susceptance of the transmission lines [5], [9], [10]. The power system operates according to nonlinear power flow equations, which are often approximated by the linearized DC model [64].

This linear model can be written as (7) with $h_M(\mathbf{L}) = \mathbf{L}$, where \mathbf{y} is the active power vector and \mathbf{x} is the unknown system state vector, both can be treated as graph signals [5], [9]. PSSE aims to estimate \mathbf{x} based on system measurements \mathbf{y} . The voltage data of power grids has been shown empirically and theoretically to be smooth/a graph LPF signal [5], [9], [63]. Thus, we model it by using $h_R^+(\mathbf{L}) = \mathbf{L}$. In addition, for state estimation to be feasible, bus 111 is set to be a reference bus with zero-phase. It is worth noting that the choice of the slack bus may influence the results, but not significantly. In the following, we use power data (susceptances and voltage angles) obtained from the IEEE 118-bus test case [34], where the noise covariance $\mathbf{R} = 0.01\mathbf{I}$ is used.

1) *Robustness to sampling set size:* Figure 2.a presents the MSE of the GFR-ML estimator versus the percentage of measured nodes, \tilde{q} , for sampling allocations based on all the proposed cost functions. The sharp decrease in MSE as \tilde{q} increases from 91% to 100% indicates the phase transition from a singular to a well-defined problem, where the number of measurements equals the number of parameters to estimate. It can be seen that for $60\% \leq \tilde{q} \leq 90\%$, all the proposed methods outperform the A-design, E-design, and LR-design. This is because methods such as A-design, E-design, and LR-design rely on the assumption that the measured signal is smooth or bandlimited, which is not satisfied in this case. The WC-MSE and bCRB achieve better performance compared to the simulation in Fig. 1a, despite using the same graph filters for $h_M(\mathbf{L})$ and h_R^+ . This difference arises because Fig. 1a considers the Bayesian case, whereas the current scenario involves non-Bayesian estimation, where the parameter corresponds to the single voltage angles vector from [34] used across all simulations, and is relatively close to the specific voltage angles assumed by these cost functions.

2) *Robustness to noise:* In Figure 2.b the MSE of the GFR-ML is presented versus $\frac{1}{\sigma^2}$ for $\tilde{q} = 70\%$ for the different sampling methods. It can be seen that all the sampling allocations are consistent, in the sense that the MSE decreases as $1/\sigma^2$ increases. It can be seen that the bCRB and the LR-design are more robust for small values of $1/\sigma^2$, whereas the WC-BMSE achieves a lower MSE for high values of $1/\sigma^2$. This highlights a tradeoff between robustness to noise and the alignment of the sampling method with the data characteristics. In this case, the noise does not contain graphical information, as $\mathbf{R} = \mathbf{I}$, which explains why the bCRB, with its reduced reliance on graphical knowledge (assuming $\mathbf{x}_0 = \mathbf{0}$), performs well in low signal-to-noise ratio (SNR) scenarios. However, at high $1/\sigma^2$ (high SNR), the fit of the sampling policy to the data becomes critical. Other sampling methods, apart from the WC-BMSE, suffer from mismatch assumptions, such as the smoothness or bandlimited nature of the measured signal (conditions not satisfied in power systems), or an inappropriate choice of \mathbf{x}_0 in bCRB and WC-MSE. Additionally, the BMSE, which averages over all eigenvalues of the Bayesian matrix in (28), is more sensitive to outliers at the high graph frequencies in comparison to the WC-BMSE, which take the largest eigenvalue.

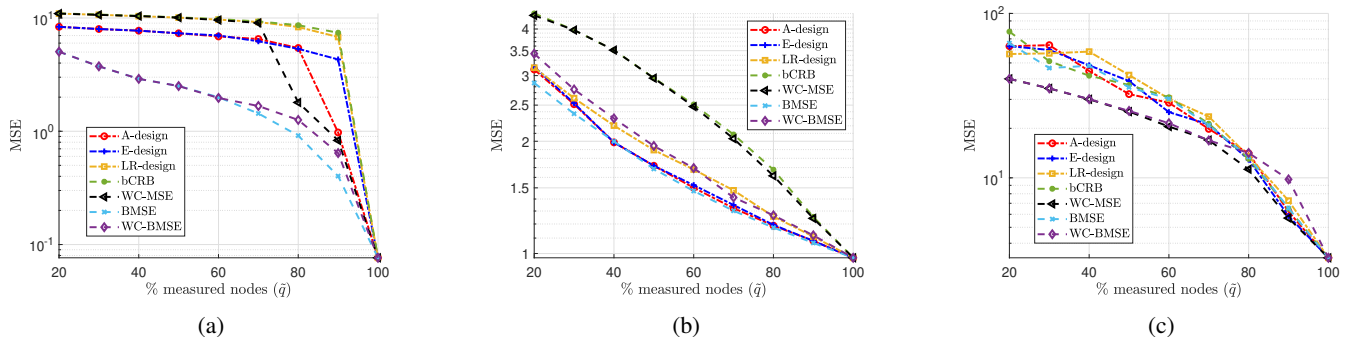


Fig. 1: The MSE versus the percentage of sampled nodes, \tilde{q} , of the different sampling sets, where the graph filters that generated the data are defined in Table I: (a) $h_M(\mathbf{L}) = \mathbf{L}$, $(h_R^+(\mathbf{L}))^\dagger = h_{\text{GMRF}}$; (b) $h_M(\mathbf{L}) = \mathbf{I}$, $(h_R^+(\mathbf{L}))^\dagger = h_{\text{Tikh}}$, $\alpha = 0.2$; and (3) $h_M(\mathbf{L}) = h_{\text{Diff}}$, $\tau = 0.5$, $h_R^+(\mathbf{L}) = \mathbf{I}$.

3) *Robustness to topology mismatches*: In Figure 2.c the MSE of the GFR-ML is presented versus the number of missing/added edges, $\Delta\mathbf{L}$, for $\tilde{q} = 70\%$. To investigate the robustness of the different methods to topology perturbations, we introduce topology mismatches, where $\Delta\mathbf{L}$ edges were randomly removed or added from the Laplacian matrix, which results in a perturbed Laplacian matrix in the sampling allocation methods and to the GFR-ML estimator. It can be seen that the bCRB, with its reduced reliance on graphical knowledge (assuming $\mathbf{x}_0 = \mathbf{0}$), is the most robust to topology mismatches. The MSE for all the other sampling sets increase as $\Delta\mathbf{L}$ increases, because they rely more on the graphical data and are dedicated to the true graph and not to the one with random changes.

C. Road Networks Data

Road networks can be represented as graphs, where nodes model locations with significant changes in traffic properties (e.g. intersections), and edges represent roads connecting these nodes [65]. In this framework, various traffic metrics, such as vehicle speed, vehicle density, and public transportation demand, can be modeled as graph signals. Due to the large scale of road networks, often spanning thousands of intersections, sensor maintenance, and data processing are computationally challenging. Sampling the network nodes provides a practical solution, that is, selecting a representative subset that retains the essential information of the original network. Studies suggest that vehicle movement in such networks often exhibits diffusion-like behavior, offering insights into urban traffic dynamics [66].

In this section, we focus on designing sampling allocation schemes that optimize the estimation performance of the GFR-ML estimator in road networks. We used the Minnesota road graph from the GSP Toolbox [35], where smooth graph signals are generated according to the model in (9) with $h_M(\mathbf{L}) = h_{\text{Diff}}$, with $\tau = 0.5$, and $h_R^+(\mathbf{L}) = h_{\text{Tikh}}$, with $\alpha = 0.01$, see Table 1). We compare the MSE of the GFR-ML estimator versus the number of nodes, \tilde{q} , for all sampling methods. Since the Minnesota road graph has $N = 2,642$ nodes, all methods are implemented using the computationally efficient PGD algorithm from Algorithm 2. Thus, the gradient of the cost function must be computed: for the A-design method [14], the implementation leverages the connection discussed in Claim 2, utilizing the gradient of the BMSE

provided in (54); for the E-design and LR-design methods, the gradient is given by (55) with $h_M(\mathbf{L})$ and $h_R^+(\mathbf{L})$ from (42), with $\mu = 10^4$ and $\mathcal{R} = \{1, \dots, N/2\}$, for the E-design [16], and $h_M(\mathbf{L}) = \mathbf{I}$ and $h_R^+(\mathbf{L}) = \mathbf{L}$ for the LR-design. The gradient derivatives of these methods, enabling their use with Algorithm 2, are a byproduct of our work.

In Fig. 3, it can be seen that the MSE decreases as the number of samples increases for all methods. For an almost fully-observable system ($q = 90\%$), the performance of the GFR-ML estimator is similar across all sampling methods. At the other extreme of sparse sampling] ($q = 20\%$), all methods yield comparable (poor) results, as the number of sensors is insufficient for accurate estimation. For $40\% \leq \tilde{q} \leq 80\%$, it can be seen that the BMSE criterion outperforms the estimation based on the A-design, E-design, and LR-design since the data is smooth, albeit not exactly bandlimited. In addition, the BMSE-based sampling outperforms the bCRB, WC-MSE, and WC-BMSE methods, because it balances flexibility and generality. Unlike the bCRB and WC-MSE, which optimize for specific values of \mathbf{x} , and the overly conservative WC-BMSE, the BMSE leverages a Bayesian prior to perform well across a wide range of \mathbf{x} , ensuring better overall performance.

VII. CONCLUSION

In this paper, we propose a comprehensive framework for efficient sampling allocation for graph signal recovery using the GFR-ML estimator. By utilizing general graph filters for both the measurement model and the regularization, the GFR-ML approach effectively enhances recovery performance in underdetermined systems. We show that its MSE depends on the unknown parameter and, thus, cannot be used as a criterion for optimization. As an alternative, we introduce four task-specific cost functions to optimize sampling allocation strategies: bCRB, WC-MSE, BMSE, and WC-BMSE. We investigate their properties and establish connections to existing methods, including A-design, E-design, and the LR approach. To address computational complexity, we developed a greedy algorithm and an alternating PGD method. Thus, the proposed methods generalize traditional bandlimited- and smoothness-based approaches, offering robust performance for a wide range of graph signal recovery tasks. Moreover, our framework does not need the actual measurements, and hence, it is well-suited for solving offline design problems. Simulation results on synthetic and real-world datasets, including the IEEE 118-bus power system and the Minnesota road network, showed

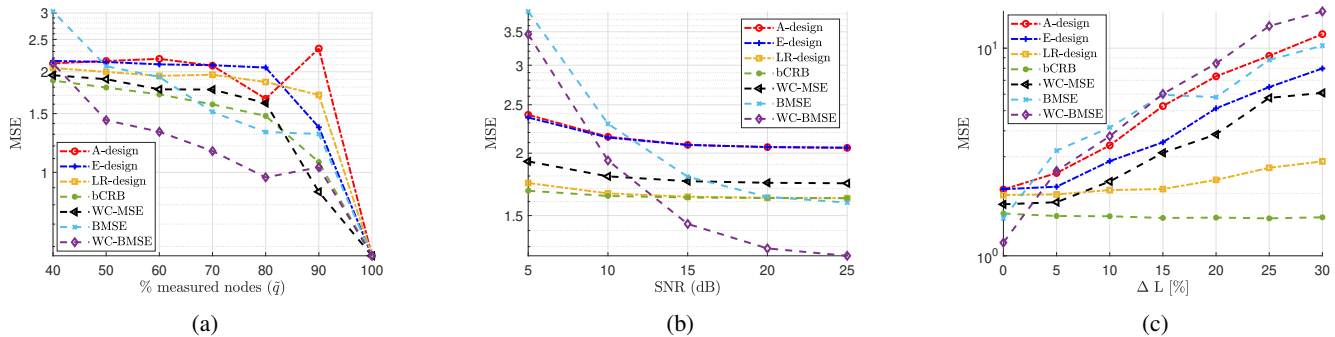


Fig. 2: State estimation in power systems: the MSE of the GFR-ML from (13) and (14) for all the sampling methods versus (a) the number of measured sensors, \tilde{q} , with $\sigma^2 = 0.01$; (b) $\frac{1}{\sigma^2}$ with $\tilde{q} = 70\%$; and (c) the number of edges that are different from the edges in the true graph, $\Delta \mathbf{L}$.

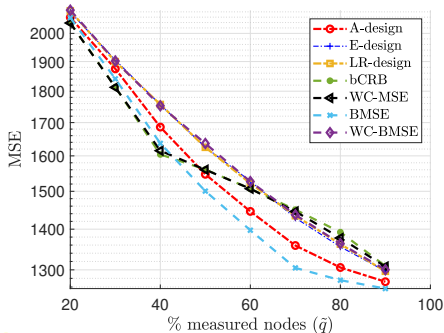


Fig. 3: The Minnesota road graph, where the graph signals are generated according to the measurement model in (9) with $h_{\mathbf{M}}(\mathbf{L}) = h_{D_{\text{diff}}}$ with $\tau = 0.5$, and $h_{\mathbf{R}}^+(\mathbf{L}) = h_{T_{\text{ikh}}}$ with $\alpha = 0.01$. The MSE versus the percentage of sampled nodes, \tilde{q} , of the different sampling sets.

substantial improvements in estimation accuracy, reducing MSE compared to existing methods. For the tested cases, the WC-MSE demonstrates the best fit for high-frequency data, the WC-BMSE and the BMSE achieve the best performance in most Bayesian settings, and the bCRB exhibits high robustness to noise and topology mismatches. Our framework demonstrated flexibility and scalability, accommodating general graph filters and enabling task-specific adaptations.

VIII. ACKNOWLEDGMENTS

The authors thank Dr. Nadav Harel, who helped during the development of the numerical example.

APPENDIX A: PROOF OF CLAIM 2

In this appendix we consider the special case described by (42). First, we simplify the BMSE matrix. By substituting $\mathbf{R} = \mathbf{I}$ and (42) in the BMSE matrix and multiplying the result by \mathbf{V}^{-1} (from left) and \mathbf{V} (from right), we obtain

$$\begin{aligned} & \mathbf{V}^{-1} \mathbf{K}(\mathbf{d}) \mathbf{V} \\ &= \text{diag}(\mathbf{1}_{\{\mathcal{R}\}}) \mathbf{V}^{-1} \mathbf{D} \mathbf{D} \mathbf{V} \text{diag}(\mathbf{1}_{\{\mathcal{R}\}}) + \text{diag}(\mu \mathbf{1}_{\{\mathcal{S} \setminus \mathcal{R}\}}). \end{aligned} \quad (58)$$

The term in (58) can be written as the block-diagonal matrix

$$\mathbf{V}^{-1} \mathbf{K}(\mathbf{d}) \mathbf{V} = \begin{pmatrix} \mathbf{V}_{\mathcal{S}, \mathcal{R}}^T \mathbf{V}_{\mathcal{S}, \mathcal{R}} & \mathbf{0} \\ \mathbf{0} & \mu \mathbf{I} \end{pmatrix}, \quad (59)$$

where we used the unitary matrix definition $\mathbf{V}^{-1} = \mathbf{V}^T$. From the pseudo-inverse properties, the pseudo-inverse of (59) can be written as

$$(\mathbf{V}^{-1} \mathbf{K}(\mathbf{d}) \mathbf{V})^\dagger = \mathbf{V}^{-1} \mathbf{K}^\dagger(\mathbf{d}) \mathbf{V} = \begin{pmatrix} (\mathbf{V}_{\mathcal{S}, \mathcal{R}}^T \mathbf{V}_{\mathcal{S}, \mathcal{R}})^\dagger & \mathbf{0} \\ \mathbf{0} & \frac{1}{\mu} \mathbf{I} \end{pmatrix}. \quad (60)$$

By using the property $\text{tr}(\mathbf{A}\mathbf{B}) = \text{tr}(\mathbf{B}\mathbf{A})$, the BMSE according to (28) can be written as

$$\text{BMSE} = \text{tr}(\mathbf{V}^{-1} \mathbf{K}^\dagger(\mathbf{d}) \mathbf{V}) = \text{tr}((\mathbf{V}_{\mathcal{S}, \mathcal{R}}^T \mathbf{V}_{\mathcal{S}, \mathcal{R}})^\dagger) + \frac{N}{\mu}, \quad (61)$$

where the second equality is obtained by substituting (60) in (28) and using the property that the trace of a block diagonal matrix is the sum of the traces of the blocks. By neglecting constant terms w.r.t. \mathcal{S} that do not influence the optimization, (61) coincides with the A-design cost function in (40).

To calculate the E-design cost function, we use the eigenvalues property $\lambda_i(\mathbf{A}^T \mathbf{A}) = \lambda_i(\mathbf{A} \mathbf{A}^T)$ to obtain $\lambda_{\min}(\mathbf{K}(\mathbf{d})) = \lambda_{\min}(\mathbf{V}^{-1} \mathbf{K}(\mathbf{d}) \mathbf{V})$. Using the fact that the eigenvalues of a block diagonal matrix are equal to the union of the eigenvalues of the blocks, we obtain, by substituting (59) in (29),

$$\begin{aligned} \text{WC-BMSE} &= (\min_i \lambda_i(\mathbf{V}^{-1} \mathbf{K}(\mathbf{d}) \mathbf{V}))^{-1} \\ &= (\min \{ \lambda_{\min}(\mathbf{V}_{\mathcal{S}, \mathcal{R}}^T \mathbf{V}_{\mathcal{S}, \mathcal{R}}), \mu \})^{-1}. \end{aligned} \quad (62)$$

Since the minimization of $\lambda_{\min}(\mathbf{A})$ equals to the maximization of $\lambda_{\min}(\mathbf{A})$, we obtain that the WC-BMSE and the E-design cost functions coincide for any $\mu \geq \lambda_{\min}(\mathbf{V}_{\mathcal{S}, \mathcal{R}}^T \mathbf{V}_{\mathcal{S}, \mathcal{R}})$.

APPENDIX B: DERIVATION OF GRADIENTS

In this appendix, we derive the gradient of the cost functions from (24), (25), (28), and (29). For simplicity, $\mathbf{K}(\mathbf{d})$ from (14), $h_{\mathbf{M}}(\mathbf{L})$, and $h_{\mathbf{R}}^+(\mathbf{L})$ are denoted as \mathbf{K} , $h_{\mathbf{M}}$, and $h_{\mathbf{R}}^+$, respectively, throughout the derivations. The order of the following subsections is structured to simplify the mathematical steps, rather than reflecting their order of use in the paper.

A. Derivation of the gradient of (28)

In order to derive the gradient of (28) w.r.t. the vector \mathbf{d} , we note that by using the linearity of derivatives, the n th component of the gradient of the BMSE w.r.t. \mathbf{d} is

$$[\nabla \text{BMSE}(\mathbf{d})]_n = \frac{\partial}{\partial d_n} \text{tr}(\mathbf{K}^{-1}) = \text{tr} \left(\frac{\partial \mathbf{K}^{-1}}{\partial d_n} \right), \quad (63)$$

$n = 1, \dots, N$, where the second equality is a known derivative formula (see Eq. (36) in [67]). From (40) in [67], we have

$$\frac{\partial \mathbf{K}^{-1}}{\partial d_n} = -\mathbf{K}^{-1} \frac{\partial \mathbf{K}}{\partial d_n} \mathbf{K}^{-1}, \quad n = 1, \dots, N. \quad (64)$$

Let \mathbf{E}_n be a diagonal matrix with n at position (n, n) and zeros elsewhere. The derivative of \mathbf{K} from (14) is (see (37) in [67])

$$\frac{\partial \mathbf{K}}{\partial d_n} = h_M (\mathbf{E}_n \mathbf{R}^{-1} \mathbf{D} + \mathbf{D} \mathbf{R}^{-1} \mathbf{E}_n) h_M. \quad (65)$$

By substituting (64) and (65) in (63) and using the identity $\text{tr}(\mathbf{A}) = \text{tr}(\mathbf{A}^T)$, we obtain:

$$\begin{aligned} \frac{\partial \mathbf{K}^{-1}}{\partial d_n} &= -2\text{tr} \left(\mathbf{K}^{-1} h_M \mathbf{E}_n \mathbf{R}^{-1} \mathbf{D} h_M \mathbf{K}^{-1} \right) \\ &= -2\text{tr} \left(\mathbf{E}_n \mathbf{R}^{-1} \mathbf{D} h_M \mathbf{K}^{-2} h_M \right), \end{aligned} \quad (66)$$

where the last equality follows from $\text{tr}(\mathbf{A}\mathbf{B}) = \text{tr}(\mathbf{B}\mathbf{A})$. Using $\text{tr}(\mathbf{E}_n \mathbf{A}) = \mathbf{A}_{n,n}$, yields (51) with \mathbf{Q} given by (54).

B. Derivation of the gradient of (24)

To compute the gradient of (24), we substitute the connection that is obtained by changing variables in (14), $h_M \mathbf{D} \mathbf{R}^{-1} \mathbf{D} h_M = \mathbf{K} - h_R^+$, in (24):

$$\text{BCRB}(\mathbf{d}) = \text{tr}(\mathbf{K}^{-2}(\mathbf{K} - h_R^+)) = \text{BMSE}(\mathbf{d}) - \text{tr}(\mathbf{K}^{-2} h_R^+). \quad (67)$$

The gradient of the bCRB from (67) is

$$\nabla \text{BCRB}(\mathbf{d}) = \nabla \text{BMSE}(\mathbf{d}) - \nabla \text{tr}(\mathbf{K}^{-2} h_R^+). \quad (68)$$

The n th component of the last term of (68) is

$$[\nabla \text{tr}(\mathbf{K}^{-2} h_R^+)]_n = \frac{\partial}{\partial d_n} \text{tr}(\mathbf{K}^{-2} h_R^+) = \text{tr} \left(\frac{\partial \mathbf{K}^{-2}}{\partial d_n} h_R^+ \right), \quad (69)$$

where the second equality is a known derivative formula (see Eq. (36) in [67]), and since $h_R^+(\mathbf{L})$ does not depend on \mathbf{d} . By using derivative rules (see (37) from [67])

$$\frac{\partial \mathbf{K}^{-2}}{\partial d_n} = \mathbf{K}^{-1} \frac{\partial \mathbf{K}^{-1}}{\partial d_n} + \frac{\partial \mathbf{K}^{-1}}{\partial d_n} \mathbf{K}^{-1}. \quad (70)$$

By substituting (64) in (70) we obtain

$$\frac{\partial \mathbf{K}^{-2}}{\partial d_n} = -\mathbf{K}^{-2} \frac{\partial \mathbf{K}}{\partial d_n} \mathbf{K}^{-1} - \mathbf{K}^{-1} \frac{\partial \mathbf{K}}{\partial d_n} \mathbf{K}^{-2}. \quad (71)$$

By substituting (71) in (69) and using the property $\text{tr}(\mathbf{A}\mathbf{B}) = \text{tr}(\mathbf{B}\mathbf{A})$ and the property $\text{tr}(\mathbf{A}) = \text{tr}(\mathbf{A}^T)$ we obtain

$$[\nabla \text{tr}(\mathbf{K}^{-2} h_R^+)]_n = -2\text{tr}(\mathbf{K}^{-2} \frac{\partial \mathbf{K}}{\partial d_n} \mathbf{K}^{-1} h_R^+). \quad (72)$$

By substituting (65) in (72) and using the property $\text{tr}(\mathbf{A}\mathbf{B}) = \text{tr}(\mathbf{B}\mathbf{A})$ and the property $\text{tr}(\mathbf{A}) = \text{tr}(\mathbf{A}^T)$ we obtain

$$\begin{aligned} &[\nabla \text{tr}(\mathbf{K}^{-2} h_R^+)]_n \\ &= -2\text{tr} \left(\mathbf{E}_n \mathbf{R}^{-1} \mathbf{D} h_M \mathbf{K}^{-1} (\mathbf{K}^{-1} h_R^+ + h_R^+ \mathbf{K}^{-1}) \mathbf{K}^{-1} h_M \right). \end{aligned} \quad (73)$$

By noting that $\text{tr}(\mathbf{E}_n \mathbf{A}) = \mathbf{A}_{n,n}$ we obtain

$$\begin{aligned} &\nabla \text{tr}(\mathbf{K}^{-2} h_R^+) \\ &= -2\text{diag} \left(\mathbf{R}^{-1} \mathbf{D} h_M \mathbf{K}^{-1} (\mathbf{K}^{-1} h_R^+ + h_R^+ \mathbf{K}^{-1}) \mathbf{K}^{-1} h_M \right). \end{aligned} \quad (74)$$

Substituting (54) into (51) to obtain $\nabla \text{BMSE}(\mathbf{d})$, and then substituting it along with (74) into (68), yields (51) with \mathbf{Q} given by (52).

C. Derivation of the gradient of (25)

In the following we derive the gradient of (25) w.r.t. \mathbf{d} . First, we note that according to (25), we have

$$\nabla \text{MSE}_{wc}(\mathbf{d}) = \nabla \text{bCRB}(\mathbf{d}) + \nabla \lambda_{\max}(h_R^+ \mathbf{K}^{-2} h_R^+). \quad (75)$$

The eigenvalue $\lambda_{\max}(h_R^+ \mathbf{K}^{-2} h_R^+)$ depends on \mathbf{d} through \mathbf{K} . The gradient of the maximal eigenvalue w.r.t. a parameter is given by (see, e.g. Eq. (67) in [67])

$$\frac{\partial \lambda_{\max}(h_R^+ \mathbf{K}^{-2} h_R^+)}{\partial d_n} = \mathbf{u}_{\max}^T h_R^+ \frac{\partial (\mathbf{K}^{-2})}{\partial d_n} h_R^+ \mathbf{u}_{\max}, \quad (76)$$

where \mathbf{u}_{\max} is the normalized eigenvector corresponding to the maximal eigenvalue, and the last equality is obtained since $h_R^+(\mathbf{L})$ is not a function of \mathbf{d} . By substituting (71) in (76) we obtain

$$\begin{aligned} &\frac{\partial \lambda_{\max}(h_R^+ \mathbf{K}^{-2} h_R^+)}{\partial d_n} \\ &= -\mathbf{u}_{\max}^T h_R^+ \mathbf{K}^{-1} \left(\mathbf{K}^{-1} \frac{\partial \mathbf{K}}{\partial d_n} + \frac{\partial \mathbf{K}}{\partial d_n} \mathbf{K}^{-1} \right) \mathbf{K}^{-1} h_R^+ \mathbf{u}_{\max} \\ &= -2\mathbf{u}_{\max}^T h_R^+ \mathbf{K}^{-2} \frac{\partial \mathbf{K}}{\partial d_n} \mathbf{K}^{-1} h_R^+ \mathbf{u}_{\max}. \end{aligned} \quad (77)$$

By substituting (65) in (77) we obtain

$$\begin{aligned} &\frac{\partial \lambda_{\max}(h_R^+ \mathbf{K}^{-2} h_R^+)}{\partial d_n} = -2\mathbf{u}_{\max}^T h_R^+ \mathbf{K}^{-2} h_M \\ &\quad \times \left(\mathbf{E}_n \mathbf{R}^{-1} \mathbf{D} + \mathbf{D} \mathbf{R}^{-1} \mathbf{E}_n \right) h_M \mathbf{K}^{-1} h_R^+ \mathbf{u}_{\max}. \end{aligned} \quad (78)$$

Since the trace of a scalar is the scalar itself, the property $\text{tr}(\mathbf{A}\mathbf{B}) = \text{tr}(\mathbf{B}\mathbf{A})$ and the property $\text{tr}(\mathbf{A}) = \text{tr}(\mathbf{A}^T)$ we obtain

$$\begin{aligned} &\frac{\partial \lambda_{\max}(h_R^+ \mathbf{K}^{-2} h_R^+)}{\partial d_n} = -2\text{tr} \left(\mathbf{E}_n \mathbf{R}^{-1} \mathbf{D} h_M \mathbf{K}^{-1} \right. \\ &\quad \times \left. (\mathbf{K}^{-1} h_R^+ \mathbf{u}_{\max} \mathbf{u}_{\max}^T h_R^+ + h_R^+ \mathbf{u}_{\max} \mathbf{u}_{\max}^T h_R^+ \mathbf{K}^{-1}) \mathbf{K}^{-1} h_M \right). \end{aligned} \quad (79)$$

By noting that $\text{tr}(\mathbf{E}_n \mathbf{A}) = \mathbf{A}_{n,n}$ we obtain

$$\begin{aligned} &\nabla \lambda_{\max}(h_R^+ \mathbf{K}^{-2} h_R^+) = -2\text{diag} \left(\mathbf{R}^{-1} \mathbf{D} h_M \mathbf{K}^{-1} \right. \\ &\quad \times \left. (\mathbf{K}^{-1} h_R^+ \mathbf{u}_{\max} \mathbf{u}_{\max}^T h_R^+ + h_R^+ \mathbf{u}_{\max} \mathbf{u}_{\max}^T h_R^+ \mathbf{K}^{-1}) \mathbf{K}^{-1} h_M \right). \end{aligned} \quad (80)$$

Substituting (52) into (51) to obtain $\nabla \text{bCRB}(\mathbf{d})$, and then substituting it along with (80) into (75), yields (51) with \mathbf{Q} given by (53).

D. Derivation of the gradient of (29)

In the following we derive the gradient of (29). First, we note that $\lambda_{\max}(\mathbf{K}^{-1}) = \lambda_{\min}^{-1}(\mathbf{K})$. The eigenvalue $\lambda_{\min}(\mathbf{K})$ depends on \mathbf{d} through \mathbf{K} . The gradient of an eigenvalue w.r.t. a parameter is given by (see, e.g. Eq. (67) in [67])

$$\frac{\partial \lambda_{\min}(\mathbf{K})}{\partial d_n} = \mathbf{u}_{\min}^T \frac{\partial \mathbf{K}}{\partial d_n} \mathbf{u}_{\min}, \quad (81)$$

where \mathbf{u}_{\min} is the normalized eigenvector corresponding to $\lambda_{\min}(\mathbf{K})$, and the last equality is obtained because h_R^+ is not a function of \mathbf{d} . By substituting (65) in (81) we obtain

$$\begin{aligned} &\frac{\partial \lambda_{\min}^{-1}(\mathbf{K})}{\partial d_n} \\ &= -\lambda_{\min}^{-2}(\mathbf{K}) \mathbf{u}_{\min}^T h_M \left(\mathbf{E}_n \mathbf{R}^{-1} \mathbf{D} + \mathbf{D} \mathbf{R}^{-1} \mathbf{E}_n \right) h_M \mathbf{u}_{\min} \\ &= -\lambda_{\min}^{-2}(\mathbf{K}) \text{tr} \left((\mathbf{E}_n \mathbf{R}^{-1} \mathbf{D} + \mathbf{D} \mathbf{R}^{-1} \mathbf{E}_n) h_M \mathbf{u}_{\min} \mathbf{u}_{\min}^T h_M \right). \end{aligned} \quad (82)$$

By using the trace operator properties, we obtain

$$\frac{\partial \lambda_{\min}^{-1}(\mathbf{K})}{\partial d_n} = -2\lambda_{\min}^{-2}(\mathbf{K}) \text{tr} \left(\mathbf{E}_n \mathbf{R}^{-1} \mathbf{D} h_M \mathbf{u}_{\min} \mathbf{u}_{\min}^T h_M \right). \quad (83)$$

Noting that $\text{tr}(\mathbf{E}_n \mathbf{A}) = \mathbf{A}_{n,n}$, yields (51) with \mathbf{Q} given by (55).

REFERENCES

- [1] M. Newman, *Networks: An Introduction*. New York, NY, USA: Oxford University Press, Inc., 2010.
- [2] D. I. Shuman, S. K. Narang, P. Frossard, A. Ortega, and P. Vandergheynst, "The emerging field of signal processing on graphs: Extending high-dimensional data analysis to networks and other irregular domains," *IEEE Signal Process. Mag.*, vol. 30, no. 3, pp. 83–98, May 2013.
- [3] A. Sandryhaila and J. M. F. Moura, "Discrete signal processing on graphs: Frequency analysis," *IEEE Trans. Signal Process.*, vol. 62, no. 12, pp. 3042–3054, June 2014.
- [4] A. Ortega, P. Frossard, J. Kovačević, J. M. F. Moura, and P. Vandergheynst, "Graph signal processing: Overview, challenges, and applications," *Proc. IEEE*, vol. 106, no. 5, pp. 808–828, May 2018.
- [5] L. Dabush, A. Kroizer, and T. Rautenberg, "State estimation in partially observable power systems via graph signal processing tools," *Sensors*, vol. 23, no. 3, p. 1387, 2023.
- [6] A. Singer and Y. Shkolnisky, "Three-dimensional structure determination from common lines in cryo-em by eigenvectors and semidefinite programming," *SIAM journal on imaging sciences*, vol. 4, no. 2, pp. 543–572, 2011.
- [7] A. Giridhar and P. R. Kumar, "Distributed clock synchronization over wireless networks: Algorithms and analysis," in *IEEE CDC*, Dec. 2006, pp. 4915–4920.
- [8] R. Ramakrishna, H. T. Wai, and A. Scaglione, "A user guide to low-pass graph signal processing and its applications: Tools and applications," *IEEE Signal Process. Mag.*, vol. 37, no. 6, pp. 74–85, 2020.
- [9] E. Drayer and T. Rautenberg, "Detection of false data injection attacks in smart grids based on graph signal processing," *IEEE Syst. J.*, vol. 14, no. 2, pp. 1886–1896, 2020.
- [10] L. Dabush and T. Rautenberg, "Detection of false data injection attacks in unobservable power systems by Laplacian regularization," *IEEE Sensor Array and Multichannel Signal Processing Workshop*, June, 2022.
- [11] G. Morgenstern, L. Dabush, J. Kim, J. Anderson, G. Zussman, and T. Rautenberg, "Invited paper: Detection of false data injection attacks in power systems using a secured-sensors and graph-based method," in *Stabilization, Safety, and Security of Distributed Systems*, S. Dolev and B. Schieber, Eds. Cham: Springer Nature Switzerland, 2023, pp. 240–258.
- [12] L. Dabush and T. Rautenberg, "Verifying the smoothness of graph signals: A graph signal processing approach," *IEEE Trans. Signal Process.*, vol. 72, pp. 4349–4365, 2024.
- [13] Y. Zhao, J. Chen, A. Goldsmith, and H. V. Poor, "Identification of outages in power systems with uncertain states and optimal sensor locations," *IEEE J. Sel. Topics Signal Process.*, vol. 8, no. 6, pp. 1140–1153, 2014.
- [14] A. Anis, A. Gadde, and A. Ortega, "Efficient sampling set selection for bandlimited graph signals using graph spectral proxies," *IEEE Trans. Signal Process.*, vol. 64, no. 14, pp. 3775–3789, 2016.
- [15] X. Wang, M. Wang, and Y. Gu, "A distributed tracking algorithm for reconstruction of graph signals," *IEEE J. Sel. Topics Signal Process.*, vol. 9, no. 4, pp. 728–740, June 2015.
- [16] S. Chen, R. Varma, A. Sandryhaila, and J. Kovačević, "Discrete signal processing on graphs: Sampling theory," *IEEE Trans. Signal Process.*, vol. 63, no. 24, pp. 6510–6523, Dec. 2015.
- [17] X. Wang, J. Chen, and Y. Gu, "Local measurement and reconstruction for noisy bandlimited graph signals," *Signal Process.*, vol. 129, pp. 119–129, December 2016.
- [18] A. G. Marques, S. Segarra, G. Leus, and A. Ribeiro, "Sampling of graph signals with successive local aggregations," *IEEE Trans. Signal Process.*, vol. 64, no. 7, pp. 1832–1843, Apr. 2016.
- [19] Y. Tanaka, Y. C. Eldar, A. Ortega, and G. Cheung, "Sampling signals on graphs: From theory to applications," *IEEE Signal Process. Mag.*, vol. 37, no. 6, pp. 14–30, 2020.
- [20] C. Dinesh, S. Bagheri, G. Cheung, and I. V. Bajić, "Linear-time sampling on signed graphs via Gershgorin disc perfect alignment," in *Proc. of ICASSP*, 2022, pp. 5942–5946.
- [21] N. Perraudin, B. Ricaud, D. I. Shuman, and P. Vandergheynst, "Global and local uncertainty principles for signals on graphs," *APSIPA Transactions on Signal and Information Processing*, vol. 7, p. e3, 2018.
- [22] S. Chen, D. Tian, C. Feng, A. Vetro, and J. Kovačević, "Fast resampling of three-dimensional point clouds via graphs," *IEEE Trans. Signal Process.*, vol. 66, no. 3, pp. 666–681, 2018.
- [23] G. Puy, N. Tremblay, R. Gribonval, and P. Vandergheynst, "Random sampling of bandlimited signals on graphs," *Applied and Computational Harmonic Analysis*, vol. 44, no. 2, pp. 446–475, 2018.
- [24] D. I. Shuman, P. Vandergheynst, and P. Frossard, "Chebyshev polynomial approximation for distributed signal processing," in *Proc. of DCOSS*, 2011, pp. 1–8.
- [25] A. Ortega, "Introduction to graph signal processing." Cambridge University Press, 2022.
- [26] S. Chen, A. Sandryhaila, and J. Kovačević, "Distributed algorithm for graph signal inpainting," in *Proc. of ICASSP*, April 2015, pp. 3731–3735.
- [27] S. Segarra, A. G. Marques, G. Leus, and A. Ribeiro, "Reconstruction of graph signals through percolation from seeding nodes," *IEEE Trans. Signal Process.*, vol. 64, no. 16, pp. 4845–4860, August 2016.
- [28] A. Kroizer, Y. C. Eldar, and T. Rautenberg, "Modeling and recovery of graph signals and difference-based signals," in *IEEE Global Conference on Signal and Information Processing (GlobalSIP)*, 2019, pp. 1–5.
- [29] K. Zhang, M. Coutino, and E. Isufi, "Sampling graph signals with sparse dictionary representation," in *Proc. of EUSIPCO*, 2021, pp. 1815–1819.
- [30] Y. Bai, F. Wang, G. Cheung, Y. Nakatsukasa, and W. Gao, "Fast graph sampling set selection using gershgorin disc alignment," *IEEE Trans. Signal Process.*, vol. 68, pp. 2419–2434, 2020.
- [31] S. Joshi and S. Boyd, "Sensor selection via convex optimization," *IEEE Trans. Signal Process.*, vol. 57, no. 2, pp. 451–462, 2009.
- [32] S. P. Chepuri and G. Leus, "Sparsity-promoting sensor selection for non-linear measurement models," *IEEE Trans. Signal Process.*, vol. 63, no. 3, pp. 684–698, 2015.
- [33] Y. Liu, L. Zhou, Q. Wei, and B. Zhao, "Sensor management based on convex optimization via prlb and joint interception probability," in *2022 IEEE Sensors*, 2022, pp. 1–4.
- [34] "Power systems test case archive." [Online]. Available: <http://www.ee.washington.edu/research/pstca/>
- [35] N. Perraudin, J. Paratte, D. Shuman, L. Martin, V. Kalofolias, P. Vandergheynst, and D. K. Hammond, "GSPBOX: A toolbox for signal processing on graphs," *ArXiv e-prints*, Aug. 2014.
- [36] S. Chen, A. Sandryhaila, J. M. F. Moura, and J. Kovačević, "Signal recovery on graphs: Variation minimization," *IEEE Trans. Signal Process.*, vol. 63, no. 17, pp. 4609–4624, Sept. 2015.
- [37] X. Zhou, S. Liu, W. Xu, K. Xin, Y. Wu, and F. Meng, "Bridging hydraulics and graph signal processing: A new perspective to estimate water distribution network pressures," *Water Research*, vol. 217, p. 118416, 2022.
- [38] R. Olfati-Saber and J. S. Shamma, "Consensus filters for sensor networks and distributed sensor fusion," in *Proceedings of the 44th IEEE Conference on Decision and Control*, Dec. 2005, pp. 6698–6703.
- [39] X. Dong, D. Thanou, L. Toni, M. Bronstein, and P. Frossard, "Graph signal processing for machine learning: A review and new perspectives," *IEEE Signal Process. Mag.*, vol. 37, no. 6, pp. 117–127, 2020.
- [40] V. Kalofolias, "How to learn a graph from smooth signals," in *Journal of Machine Learning Research (JMLR)*, 2016, pp. 920–929.
- [41] J. Hara, Y. Tanaka, and Y. C. Eldar, "Graph signal sampling under stochastic priors," *IEEE Trans. Signal Process.*, vol. 71, pp. 1421–1434, 2023.
- [42] T. Rautenberg, "Non-Bayesian estimation framework for signal recovery on graphs," *IEEE Trans. on Signal Process.*, vol. 28, pp. 175–179, 2021.
- [43] P. M. Djuric and C. Richard, *Sampling and Recovery of Graph Signals*. Academic Press, 2018, ch. 9.
- [44] S. Chen, R. Varma, A. Singh, and J. Kovačević, "Signal recovery on graphs: Fundamental limits of sampling strategies," *IEEE Trans. Signal Inf. Process. Netw.*, vol. 2, no. 4, pp. 539–554, 2016.
- [45] L. O. B. Le Bars, P. Humbert and A. Kalogeratos, "Learning Laplacian matrix from bandlimited graph signals," *IEEE International Conference on Acoustics, Speech and Signal Processing (ICASSP)*, Brighton, United Kingdom 2019, pp. 2937–2941, 2019.
- [46] X. Dong, D. Thanou, P. Frossard, and P. Vandergheynst, "Learning Laplacian matrix in smooth graph signal representations," *IEEE Trans. Signal Process.*, vol. 64, no. 23, pp. 6160–6173, Dec. 2016.
- [47] M. Ramezani-Mayami, M. Hajimirsadeghi, K. Skretting, R. S. Blum, and H. V. Poor, "Graph topology learning and signal recovery via Bayesian inference," in *DSW*, 2019, pp. 52–56.
- [48] W. N. van Wieringen, "Lecture notes on ridge regression," 2015. [Online]. Available: <https://arxiv.org/abs/1509.09169>
- [49] A. Chiumento, N. Marchetti, and I. Macaluso, "Energy efficient wsn: a cross-layer graph signal processing solution to information redundancy," in *2019 16th International Symposium on Wireless Communication Systems (ISWCS)*, 2019, pp. 645–650.
- [50] S. M. Kay, *Fundamentals of statistical signal processing: Estimation Theory*. Englewood Cliffs (N.J.): Prentice Hall PTR, 1993, vol. 1.
- [51] A. O. Hero, J. A. Fessler, and M. Usman, "Exploring estimator bias-variance tradeoffs using the uniform cr bound," *IEEE Trans. Signal Process.*, vol. 44, no. 8, pp. 2026–2041, 1996.

- [52] Y. C. Eldar, "Minimum variance in biased estimation: Bounds and asymptotically optimal estimators," *IEEE Trans. Signal Process.*, vol. 52, no. 7, pp. 1915–1930, 2004.
- [53] R. A. Horn and C. R. Johnson, *Matrix Analysis*, 2nd ed. New York, NY, USA: Cambridge University Press, 2012.
- [54] F. Amin, O. M. Barukab, and G. S. Choi, "Big data analytics using graph signal processing," *Computers, Materials and Continua*, vol. 74, no. 1, pp. 489–502, 2022.
- [55] D. P. Bertsekas, *Nonlinear Programming*, 2nd ed. Athena Scientific, 1999.
- [56] S. Boyd and L. Vandenberghe, *Convex Optimization*. New York, NY, USA: Cambridge University Press, 2004.
- [57] S. Boyd and J. Dattorro, "Alternating projections," *EE392o, Stanford University*, 2003.
- [58] E. Isufi, F. Gama, D. I. Shuman, and S. Segarra, "Graph filters for signal processing and machine learning on graphs," *IEEE Trans. Signal Process.*, pp. 1–32, 2024.
- [59] N. L. R. Y. Bengio, O. Delalleau, *Semi-Supervised Learning*. United States of America: Massachusetts Institute of Technology, 2006.
- [60] D. Thanou, X. Dong, D. Kressner, and P. Frossard, "Learning heat diffusion graphs," *IEEE Trans. Signal Inf. Process. Netw.*, vol. 3, no. 3, pp. 484–499, 2017.
- [61] R. Pena, X. Bresson, and P. Vandergheynst, "Source localization on graphs via l1 recovery and spectral graph theory," in *2016 IEEE 12th Image, Video, and Multidimensional Signal Processing Workshop (IVMSP)*, 2016, pp. 1–5.
- [62] C. Ye and G. Mateos, "Learning to identify sources of network diffusion," in *Proc. of EUSIPCO, 2022*, pp. 727–731.
- [63] R. Ramakrishna and A. Scaglione, "Grid-graph signal processing (grid-GSP): A graph signal processing framework for the power grid," *IEEE Trans. Signal Process.*, vol. 69, pp. 2725–2739, 2021.
- [64] G. B. Giannakis, V. Kekatos, N. Gatsis, S. J. Kim, H. Zhu, and B. F. Wollenberg, "Monitoring and optimization for power grids: A signal processing perspective," *IEEE Signal Process. Mag.*, vol. 30, no. 5, pp. 107–128, Sept. 2013.
- [65] U. Demiryurek, B. Pan, F. Banaei-Kashani, and C. Shahabi, "Towards modeling the traffic data on road networks," in *Proc. of IWCTS*. New York, NY, USA: Association for Computing Machinery, 2009, p. 13–18.
- [66] P. Medina, S. C. Carrasco, M. S. Jofré, J. Rogan, and J. A. Valdivia, "Characterizing diffusion processes in city traffic," *Chaos, Solitons & Fractals*, vol. 165, p. 112846, 2022.
- [67] K. B. Petersen and M. S. Pedersen, "The matrix cookbook," *Techn. Univ. Denmark*, vol. 7, no. 15, p. 510, 2012.